

Mineral layers around coarse-grained, Ca-Al-rich inclusions in CV3 carbonaceous chondrites: Formation by high-temperature metasomatism

Alex Ruzicka¹

Department of Planetary Sciences, University of Arizona, Tucson

Abstract. Coarse-grained (Type A, B) Ca-Al-rich inclusions (CAIs) in carbonaceous chondrites typically are surrounded by thin mineral layers ("rims") that have puzzled researchers for two decades. Quantitative reaction-diffusion models can account for the overall mineral zoning structures of rims and the major-element zoning of the ubiquitous clinopyroxene layer, suggesting that the layers formed by metasomatism. Melilite-bearing CAIs appear to have reacted with an external medium that primarily contained Mg-Si-rich vapor (with atomic $Mg/[Mg+Si] \leq 0.66$) and forsteritic olivine. Different reactant compositions in the external medium appear to have been largely responsible for producing different rim types. Various rims formed either in different local environments or at different times in an evolving system. It is suggested that layer formation occurred in a nebular setting, while silicates were being vaporized and olivine was condensing around CAIs. Steady state layer growth models do not adequately explain the presence of melilite layers or patches in some rims and consistently underestimate the spinel/clinopyroxene ratios of rims, probably because of a failure to attain complete steady state conditions as a result of changing pressure, temperature, or reactant compositions during layer growth. Roughly 3-50% of the spinel in rims can be attributed to metasomatic growth, but the remaining spinel formed by another process, possibly as a residue of partial melting during a brief vaporization event, or by preferential nucleation on the surfaces of molten CAIs. The thermal events accompanying CAI metasomatism can be constrained by modeling Mg isotope exchange that occurred between some CAIs and the external medium. Based on one well-studied CAI, it is inferred that isotopic exchange and layer formation was initiated either in a high-temperature ($>1450^{\circ}\text{C}$) heating event <10 hours in duration, or at lower temperatures ($\leq 1450^{\circ}\text{C}$) during cooling at a rate of $\leq 0.1\text{-}2^{\circ}\text{C/hr}$.

Introduction

Ca-Al-rich inclusions (CAIs) are an important class of centimeter- and millimeter-sized objects commonly found in carbonaceous chondrites. They have among the oldest radiometric ages measured for any solar system material, often show isotopic anomalies, and are enriched in refractory elements, suggesting that they formed early in solar system history at high temperatures, either as condensates or as vaporization residues [Tilton, 1988; Lee, 1988; MacPherson *et al.*, 1988]. The margins of coarse-grained CAIs are usually surrounded by multiple mineral layers that form "rim" sequences, typically $<50\ \mu\text{m}$ in total thickness [MacPherson *et al.*, 1988]. These layers clearly formed before the final agglomeration of the host meteorites, as the rim layers are often brecciated or displaced [Wark and Lovering, 1977; Grossman, 1980; Ruzicka and Boynton, 1992]. The layers did not form during late parent body metamorphism, but rather in the solar nebula or possibly in an early episode of parent body processing. They potentially record important information on processes that affected refractory material in the earliest moments of solar system history.

The interiors of the CAIs are composed primarily of melilite ($\text{Ca}_2\text{Al}_2\text{SiO}_7\text{-Ca}_2\text{MgSi}_2\text{O}_7$), with variable amounts of spinel ($(\text{Mg,Fe})\text{Al}_2\text{O}_4$), clinopyroxene ($\text{CaMgSi}_2\text{O}_6\text{-CaAl}_2\text{SiO}_6\text{-CaTi}^{3+}\text{AlSiO}_6\text{-CaTi}^{4+}\text{Al}_2\text{O}_6$), perovskite (CaTiO_3), and anorthite ($\text{CaAl}_2\text{Si}_2\text{O}_8$), while the rim layers are composed of zoned clinopyroxene, and various proportions of spinel, olivine ($(\text{Mg,Fe})_2\text{SiO}_4$), anorthite, melilite, and perovskite. Layer-forming clinopyroxene is consistently zoned radial to the CAIs, with Al and sometimes Ti decreasing, and Si and Mg increasing, away from the CAIs [e.g., Wark and Lovering, 1977; Ruzicka, 1996]. Four types of layer sequences are present around coarse-grained CAIs in the Leoville, Vigarano, and Efremovka CV3 chondrites (Figure 1) [Ruzicka, 1996]. There is no obvious tendency for these rim types to be strongly correlated with the mineralogy of the CAIs [Ruzicka, 1996]. These different sequences represent variations on a theme, in which layer-forming spinel, anorthite, clinopyroxene, and olivine tend to be concentrated progressively further from the CAIs.

Most CAIs and CAI rims in Leoville, Vigarano, and Efremovka show less evidence for the Fe^{2+} -alkali-halogen alteration that widely affected similar components in the Allende (CV3) chondrite [McSween, 1977; Wark and Lovering, 1977; MacPherson *et al.*, 1981, 1988; Ruzicka, 1996]. For example, feldspathoids and Fe-rich phases such as hedenbergite and andradite, common in Allende CAI rims [Wark and Lovering, 1977], are minor or absent in most CAI rims from Leoville, Vigarano, and Efremovka [Davis *et al.*, 1987; MacPherson *et al.*, 1988; Ruzicka, 1996]. Spinel and olivine in rims from the latter

¹Now at Planetary Geosciences Institute, Department of Geological Sciences, University of Tennessee, Knoxville

Copyright 1997 by the American Geophysical Union.

Paper number 97JE00416.
0148-0227/97/97JE-00416\$09.00

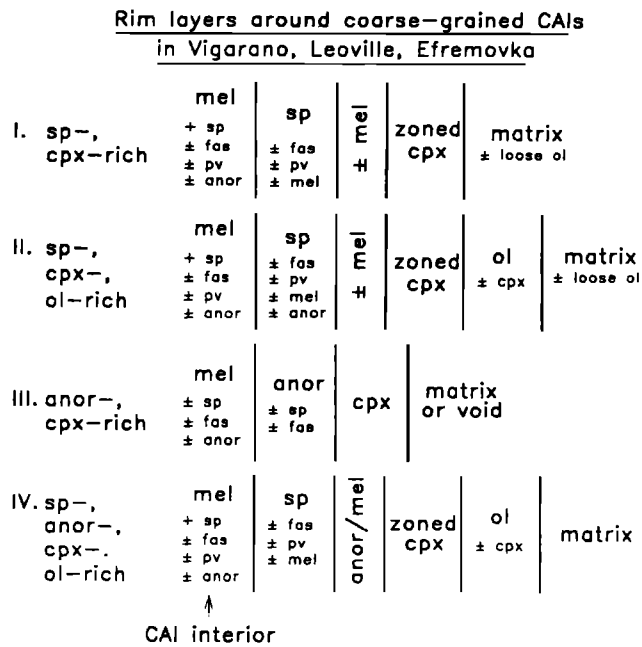


Figure 1. Schematic illustration of the major rim types around coarse-grained CAIs in Vigarano, Leoville, and Efremovka. Phases are listed in approximate order of decreasing abundance within zones. Abbreviations: mel, melilite; sp, spinel; fas, fassaite clinopyroxene; cpx, zoned clinopyroxene (chiefly Al-diopside, also fassaite, diopside); pv, perovskite; anor, anorthite; ol, forsteritic olivine. "Loose ol" refers to individual olivine grains that appear to have accreted onto the surfaces of CAIs.

three meteorites typically have Mg/(Mg+Fe) (or Mg#) atom ratios of ~0.97-1 and ~0.9-1, respectively, although the margins of some zoned olivine grains, adjacent to host matrix, have Mg# values as low as ~0.74 [Ruzicka, 1996], and these may have suffered some late alteration. Rim feldspar is close to pure anorthite ($\geq An_{97}$, mol%) in composition [Ruzicka, 1996]. This suggests that CAI rim layers did not originally form as a by-product of Fe²⁺-alkali alteration of CAI interiors [Davis *et al.*, 1987; MacPherson *et al.*, 1988; Ruzicka, 1996].

Three processes were probably important for producing rims. These include (1) flash heating, a brief, intense heating episode that created a refractory-element-enriched residue on the margins of coarse-grained CAIs [Boynton and Wark, 1984, 1985, 1987; Wark and Boynton, 1987; Wark *et al.*, 1988; Murrell and Burnett, 1987]; (2) metasomatism, involving an influx of Si and Mg into CAIs from their surroundings (external medium) [Wark and Boynton, 1987; Wark *et al.*, 1988], and/or an outflux of Ca from CAIs [MacPherson *et al.*, 1981], with some layers being produced by a coupled reaction-diffusion mechanism; and sometimes (3) grain accretion, which involved the accumulation of olivine grains and fine-grained matrix-like material onto CAI surfaces [Ruzicka and Boynton, 1993; Ruzicka, 1996]. Flash heating clearly preceded metasomatism and grain accretion, but the timing of metasomatism relative to grain accretion is unclear.

In this paper, quantitative reaction-diffusion models are used to address the following questions. (1) Is it possible to form all or some rim layers by metasomatism? (2) If so, what was the character/composition of the external medium that reacted with the CAIs? (3) What accounts for the differences between the four major types of rim layer assemblages (Figure 1)? (4) Why are

phases that are predicted to have been present in rims immediately following the putative flash heating event (e.g., refractory glass or Ca-aluminate minerals such as CaAl₂O₄) almost never observed in rims? (5) What constraints can be obtained for the timescale of metasomatism?

It is stressed that the metasomatism model for CAI rims described in this paper is analogous to that of MacPherson *et al.* [1981], except that it does not involve low-temperature, Fe²⁺-alkali-halogen alteration of the sort envisioned for Allende by these researchers. It is entirely conceivable, perhaps likely, that low-temperature alteration of CAIs in Allende and other "oxidized" CV3 chondrites [McSween, 1977] was preceded by high-temperature metasomatism, and that prior to low-temperature alteration, CAI rims in Allende resembled those in the "reduced" CV3 chondrites [McSween, 1977] Leoville, Vigarano, and Efremovka.

Layer-Growth Model

In the layer-growth model, the five cations, Mg²⁺, Al³⁺, Ca²⁺, Si⁴⁺, and Ti⁴⁺, are assumed to have diffused independently, and O²⁻ is assumed to be a dependent component. This is mathematically equivalent to assuming that diffusion occurred as the oxide species, MgO, Al₂O₃, CaO, SiO₂, and TiO₂. These are the most abundant oxide species in CAI rims from Leoville, Vigarano, and Efremovka. For reaction to occur in a five-component system, at least six phases must be present. From the phase rule, a system at constant pressure and temperature with six or more phases and five components cannot be in equilibrium, and such a system will tend to react so as to eliminate thermodynamic incompatibilities. If an unlimited supply of the phases is present, then one or more mineral layers will be produced that physically separate the incompatible phases. All reactions are assumed to occur at layer contacts only, although this assumption does not significantly affect the major results of the models [Ruzicka, 1996]. Diffusion is assumed to occur through a diffusion medium that could be a zone of crystalline disorder in minerals, an adsorbed fluid or film on grain boundaries, or any fast diffusive pathway of negligible volume compared to the bulk reacting phases.

The overall rim configuration in the models is CAI | rim | external medium, where rim = one or more (monomineralic or polymineralic) mineral layers. CAI interiors were assumed to consist of the chief phases present in most coarse-grained CAIs, namely, melilite, spinel, and either fassaite or perovskite. The external medium was assumed to consist of either (1) vapor alone, (2) vapor + olivine (forsterite), (3) vapor + clinopyroxene (Al-diopside), (4) vapor + anorthite, or (5) olivine (forsterite) + clinopyroxene (Al-diopside). An external medium that consists solely of vapor is used to model the situation in which CAIs are reacting with nebular gas, while an external medium that consists of olivine + clinopyroxene is used to model the situation in which CAIs are reacting with "dusty," matrix-like material (the matrix of carbonaceous chondrites consists chiefly of olivine and clinopyroxene). Other vapor + solid combinations are used to model the reaction of the CAIs with surrounding gas and "dust" that has accreted onto the surfaces of the CAIs. A variety of phases were included in rims, including those that are observed in rims, and those (such as refractory glass and Ca-aluminate) that may have been present immediately after a flash heating event (Table 1). Phase compositions were assumed to be constant. For vapor, both solar and nonsolar compositions were assumed (Table 1). Two compositions were assumed for refractory residues, one

Table 1. Abbreviations and Compositions for Phases Assumed in Quantitative, Five-Component (Mg-Al-Ca-Si-Ti) Models of CAI Rim Formation

Phase	Abbreviation	Composition (Atomic)
Melilite	mel	$\text{Ca}_2\text{Al}_{1.8}\text{Mg}_{0.1}\text{Si}_{1.1}\text{O}_7$ [Ak_{10}]
Spinel	sp	MgAl_2O_4
Perovskite	pv	CaTiO_3
Fassaite *	fas	$\text{Ca}_{0.9989}\text{Mg}_{0.5320}\text{Al}_{0.2602}\text{Ti}_{0.2188}\text{Si}_{1.3906}\text{Al}_{0.6015}\text{O}_6$
Al-diopside *	diop	$\text{Ca}_{0.9525}\text{Mg}_{0.9505}\text{Al}_{0.0830}\text{Ti}_{0.0120}\text{Si}_{1.8942}\text{Al}_{0.1058}\text{O}_6$
Olivine	ol	Mg_2SiO_4
Anorthite	anor	$\text{CaAl}_2\text{Si}_2\text{O}_8$
Ca-aluminate †	CA	CaAl_2O_4
Glass ‡	G	$\text{Mg}_{0.0004}\text{Al}_{0.6068}\text{Ca}_{0.3636}\text{Si}_{0.0072}\text{Ti}_{0.0220}$ (when CA absent)
Glass ‡	G	$\text{Mg}_{0.0007}\text{Al}_{0.5364}\text{Ca}_{0.3891}\text{Si}_{0.0133}\text{Ti}_{0.0405}$ (when CA present)
Vapor (Solar) **	V	$\text{Mg}_{0.4744}\text{Al}_{0.0386}\text{Ca}_{0.0272}\text{Si}_{0.4587}\text{Ti}_{0.0011}$
Vapor (Nonsolar)	V	$\text{Mg}_{0.1}\text{Al}_0\text{Ca}_0\text{Si}_{1.0}\text{Ti}_0$

* The composition for fassaite and Al-diopside are the mean compositions for fassaite within and for Al-diopside around coarse-grained (Type A, B) CAIs in the Vigarano, Leoville, and Efremovka chondrites [Ruzicka, 1996].

† Likely liquidus phase for a typical vaporization residue of coarse-grained CAIs [Ruzicka, 1996].

‡ Corresponds to a hypothetical vaporization residue produced by 80% vaporization of an average coarse-grained CAI composition [Ruzicka, 1996] containing either glass only or a 50-50 mixture of glass and CaAl_2O_4 .

** Mean CI-chondrite composition of Anders and Grevesse [1989].

corresponding to a representative glass vaporization residue, and the other to a 50-50 mixture (by mass) of glass + CaAl_2O_4 . The latter phase is likely to have been a major constituent of any crystalline CAI vaporization residue [Ruzicka, 1996].

The most critical assumptions of the model are that local equilibrium is maintained and that a quasi steady state is achieved. The former assumption requires that all phases in local contact with one another are in equilibrium, even though disequilibrium must be present on a larger scale in order for layers to form. This local equilibrium assumption is reasonable on theoretical grounds [Fisher and Elliot, 1974; Fisher, 1978]. In quasi steady state diffusion, the modes and relative thicknesses of layers do not change with time even though the actual thicknesses increase. In other words, the relative reaction rates of all phases at all layer contacts will be time-invariant, although at constant temperature the absolute reaction rates will steadily decrease with time as the structure grows and the chemical potential gradients driving diffusion diminish. A steady state can be achieved only if the initial reactants (in the CAI and external medium) do not change composition and are not fully consumed by reaction, and only if the pressure and temperature (and hence the conditions of equilibrium and the diffusion rates of the components) are not changing too rapidly [Fisher and Elliot, 1974; Fisher, 1978]. It is unclear whether a steady state would have been achieved for the metasomatic growth of rim layers.

The fluxes of components across layers are assumed to be described by

$$J_i = L_{ii} \cdot (-\nabla\mu_i) \quad (1)$$

where J_i is the flux of component i , $\nabla\mu_i$ is the chemical potential gradient of component i , and L_{ii} is an Onsager diffusion coefficient for component i [Katchalsky and Curran, 1965; Fisher, 1973, 1977; Joesten, 1977]. Both J_i and L_{ii} are measured with respect to an inert marker reference frame [Hartley and Frank,

1949; Fisher, 1977]. Implicit in this description of diffusion is that the flux of a component depends only on the chemical potential gradient of the same component, which in an inert marker frame should be correct to first order [Katchalsky and Curran, 1965, pp. 90-91; Brady, 1975]. At constant pressure and temperature, the phase assemblage and composition of the phases in each of the layers constrain the permissible values of $\nabla\mu_i$, and these, in turn, constrain the relative diffusive fluxes across layers if local equilibrium is maintained [e.g., Fisher, 1973, 1977; Joesten, 1977, 1991].

In the models, the L_{ii} values must be specified, either in a relative sense as L coefficient ratios ("L ratios") or in an absolute sense. These L coefficients represent generalized, effective mobilities of the components [Katchalsky and Curran, 1965; Brady, 1975]. In principle, their values can be determined experimentally, but as these values potentially depend on a large number of uncertain variables (such as the composition of the diffusing medium, the diffusion mechanism, temperature, $f\text{O}_2$, and pressure), the approach used here instead assumes a range of plausible L ratio values. Some important model results (such as net or overall reactions) do not depend on L ratio values, while others (such as relative layer widths, layer modes, and layer sequences) do depend on them.

The calculation procedure that was used for modeling rim layer growth involves two basic steps: (1) determination of the exchange cycle for an assumed layer sequence, and (2) incorporating the effects of reactant composition on layer growth. These basic steps are discussed in more detail below and by Ruzicka [1996].

Exchange cycle calculation. The first step is to assume a layer sequence and determine the exchange cycle, which describes the production or removal rates of all phases and diffusing components at all layer contacts. The analytical procedure is similar to that previously employed [Fisher, 1977; Joesten, 1977; Fisher and Lasaga, 1981; Nishiyama, 1983; Ashworth and Birdi, 1990]. The exchange cycle is determined by simultaneously solving a set of (1) local mass balance equations, (2) steady-flux/conservation equations, (3) steady-flux/local-equilibrium equations, and (4) "additional" equations.

Local mass balance equations (one equation for each component at each contact) simply describe mass balance between the exchange or diffusion medium and the coexisting solids at each layer contact. These equations can be expressed as

$$v_i^q = -\sum_{\phi=1}^p N_i^\phi \cdot v_\phi^q \quad (2)$$

where v_i^q is the addition (>0) or removal (<0) rate of component i from the diffusion medium at the q th contact, v_ϕ^q is the formation (>0) or dissolution (<0) rate of phase ϕ by reaction at the q th contact, N_i^ϕ is the atom proportion of component i in phase ϕ , and p is the number of phases at the q th contact.

The steady-flux/conservation equations (one equation for each component) are essentially mass balance equations for the entire system (layer assemblage + initial reactants) that take into account closed- or open-system fluxes. These equations are given by

$$J_i^{z-1} - J_i^{z \rightarrow} + \sum_{q=1}^z v_i^q / \alpha^q = 0 \quad (3)$$

where J_i^{z-1} and $J_i^{z \rightarrow}$ represent quasi steady state fluxes of component i in the initial reactants, α^q is the effective reaction area normal to diffusive flow at the q th layer contact (assumed here to have the same value at all layer contacts), and z is the number of layer contacts. J_i^{z-1} is the flux of component i in the

initial reactant adjacent to, and toward, the $q = 1$ layer contact, whereas $J_i^{z \rightarrow}$ represents the flux of i in the initial reactant adjacent to, and away from, the $q = z$ layer contact. For "open-system" diffusion, defined as involving diffusion between the system and one or more unspecified phases external to the system, $J_i^{z \rightarrow} \neq 0$ and/or $J_i^{1 \rightarrow} \neq 0$, whereas for "closed-system" diffusion, involving diffusion only between the specified phases in the models, these fluxes are zero. For open-system models, the steady state inflow or outflow rates of components must be specified. Most of the calculations reported here assumed closed-system diffusion.

The steady-flux/local-equilibrium equations (one equation for each diffusing component in each layer) describe the steady state rate at which components are transported through layers, subject to the constraint of local equilibrium between the diffusion medium and the coexisting phases in the layers. These equations can be expressed as

$$\sum_{i=1}^k N_i^\dagger L_{\text{SiSi}}/L_H \cdot \left(\sum_{m=1}^q v_i^m / \alpha^m + J_i^{z \rightarrow} \right) = 0 \quad (4)$$

where L_{SiSi}/L_H is the ratio of a reference L coefficient (e.g., L_{SiSi}) to another L coefficient, and k is the number of independent diffusing components.

One or more additional equations must also be included in the set of simultaneous equations to determine the exchange cycle. In the models for CAI rims, one such equation is used. Namely, it is assumed that SiO_2 is evolved at the rim-external medium contact at the rate of 1 mole per unit time (i.e., $v_{\text{SiO}_2}^{\text{rim-ext.med.}} = +1$). This assumption ensures that SiO_2 will diffuse from the external medium to the CAI, and implicitly assumes that the value of μ_{SiO_2} is higher in the external medium than in the CAI. This is reasonable because rims are enriched in SiO_2 relative to CAI interiors [Ruzicka and Boynton, 1994; Ruzicka, 1996], and for a metasomatic model, this can only occur if Si diffused toward CAIs into rims from the external medium. All reaction rates in this paper are therefore scaled to the production of 1 mole per unit time of SiO_2 at the rim-external medium contact. This additional equation is the only "thermochemical" input in the models. Its sign has the important effect of determining which phases will be products and which reactants in the overall or net layer-forming reactions.

Incorporating the effects of reactant composition. The modal abundances of the initial reactants play an important role in determining the stability of any particular layer sequence to steady state diffusion [Joesten, 1977; Foster, 1981, 1991; Swapp, 1988; Ruzicka, 1996]. Once the exchange cycle is calculated, the second step is to use this information together with the specified modal abundances of the initial reactants to determine (1) the modal abundances and relative (or absolute) thicknesses of each of the layers, and (2) whether the layer sequence is stable to steady state diffusion. For this step, the procedure of Ruzicka [1996] was followed.

Before giving expressions for layer modes and thicknesses, it is necessary to distinguish between the two bounding contacts of each layer. The "leading" contact will be the first of the two contacts to sweep by any given inert marker, and the "trailing" contact will follow thereafter. All mineralogically distinct layers, with one exception, will have one leading and one trailing contact that appear to move in the same direction in an inert marker frame. The exception is a layer that has two leading contacts that will appear to move in opposite directions in an inert marker frame. The latter layer can be subdivided into two mineralogically identical, but possibly modally distinct zones, with an interface

between the two that corresponds to the location of an inert marker. No reactions occur at the latter interface.

It is useful also to consider the presence of three types of phases at each layer contact. These include (1) "disappearing phases," which appear on one side of a layer contact only, and which have negative growth rates ($v_\phi^q < 0$); (2) "newly appearing phases," which appear on one side of a layer contact only, and which have positive growth rates ($v_\phi^q > 0$); and (3) "common phases," which appear on both sides of a layer contact, and which have either positive growth rates, or negative growth rates insufficient to completely remove the phase. Generally, there is only one disappearing phase at each contact.

The mode of any zone must be determined before its thickness can be calculated. The mode of a zone is controlled by (1) the reaction occurring at the leading contact of the zone, and by (2) the composition of the adjacent layer, next to the leading contact, out of which the given zone is forming. The molar fraction of phase ϕ in a mineral zone is given by

$$X_\phi^{\text{zone}} = \frac{v_\phi^L - v_d^L \cdot (X_\phi^*/X_d^*)}{\sum_{\phi=1}^p v_\phi^L - v_d^L \cdot (X_\phi^*/X_d^*)} \quad (5)$$

where v_d^L is the reaction coefficient for the disappearing phase at the leading contact, v_ϕ^L is the reaction coefficient for any newly appearing or common phase at the leading contact, X_ϕ^* is the mole fraction of any common phase in the adjacent layer, next to the leading contact, X_d^* is the mole fraction of the disappearing phase in the adjacent layer, next to the leading contact, and p is the number of phases in the zone.

The growth rate (W^{zone}), or width per unit time, of a mineral zone is found from

$$W^{\text{zone}} = \left\{ 1/\alpha^L \cdot \sum_{\phi=1}^p V_\phi \cdot (v_\phi^L - v_d^L (X_\phi^*/X_d^*)) \right\} - \left\{ 1/\alpha^T \cdot \sum_{\phi=1}^p V_\phi \cdot v_d^T (X_\phi^{\text{zone}}/X_d^{\text{zone}}) \right\} \quad (6)$$

where V_ϕ is the molar volume of phase ϕ , the superscripts L and T refer to leading (L) and trailing (T) contacts of the zone, X_ϕ^{zone} is the mole fraction of any phase in the zone, X_d^{zone} is the mole fraction of the phase in the zone that is the disappearing phase at the trailing contact, and other symbols are the same as in (5). A stable zone sequence must have $W^{\text{zone}} > 0$ for each zone.

For stable quasi steady state zone sequences, the magnitude of the reaction coefficients of diffusing components at each layer contact can be related to the magnitude of the changes in chemical potential (μ_i) gradients at each layer contact, and these in turn, can be used together with the relative thicknesses of layers to calculate relative variations in μ_i across layers [Ruzicka, 1996]. Such predicted variations in μ_i can be compared with observed concentration profiles in the phases to serve as a check on the validity of the model [e.g., Ruzicka et al., 1994]. Important in this regard is the observed zoning of clinopyroxene in rims. As components diffuse from high to low μ_i , the diffusion directions for each component within each layer can be determined.

Net (Overall) Reactions Responsible for Producing Rim Layers

An analysis of net reactions for various model systems can be used to assess what kinds of rim assemblages will be produced in different systems. Net reactions for the most relevant model rim

Table 2a. Net Reactions for Selected Five-Component (Mg-Al-Ca-Si-Ti), Six-phase Systems Possibly Relevant to the Petrogenesis of Type I and Type II Rims

Vapor Composition		
Mg/[Mg+Si] (Atomic)	Solar?	Net Reaction (Schematic)
<i>Phases: mel + sp + fas + diop + ol + V</i>		
0.51	yes	mel + fas + V → sp + diop + ol
0-0.47	no	mel + fas + V + ol → sp + diop
0.48-0.66	no	mel + fas + V → sp + diop + ol
0.67-1.00	no	mel + fas + ol → sp + diop + V
<i>Phases: mel + sp + pv + diop + ol + V</i>		
0.51	yes	mel + pv + V → sp + diop + ol
0-0.47	no	mel + pv + V + ol → sp + diop
0.48-0.66	no	mel + pv + V → sp + diop + ol
0.67-1.00	no	mel + pv + ol → sp + diop + V

Phase abbreviations and compositions are given in Table 1. Reactions assume closed-system diffusion and a relatively low value for μ_{SiO_2} in a melilite-bearing CAI assemblage.

systems undergoing closed-system diffusion are summarized in Table 2. Additional net reactions for other model rim systems are discussed by Ruzicka [1996].

It is important to note that net reactions do not depend on the values of L coefficients, the modal compositions of the reactants, or the details of the layer structures, but do depend on (1) the compositions of the phases assumed (Table 1), (2) the assumption that μ_{SiO_2} is higher in the external medium than in CAIs, and (3) whether closed- or open-system diffusion is occurring. Any representative layer sequence containing the phases of interest can be used to calculate the net reaction (whether or not the sequence is stable to quasi steady state diffusion). This type of modeling, considering net reactions only, essentially represents a sophisticated way to balance reactions in a specified system. As net reactions depend on few uncertain parameters or assumptions, inferences derived from them are relatively robust. However, an analysis of net reactions alone cannot demonstrate whether the layer sequences, widths, or modes of layer assemblages can be successfully modeled (see next section), but only whether certain phases will appear in the layers.

Table 2b. Same as for Table 2a, Except for Systems Possibly Relevant to the Petrogenesis of Type III Rims

Vapor Composition		
Mg/[Mg+Si] (Atomic)	Solar?	Net Reaction (Schematic)
<i>Phases: mel + sp + fas + diop + anor + V</i>		
0.51	yes	sp + diop → mel + fas + anor + V
0-0.27	no	mel + sp + fas + V → anor + diop
0.28-0.47	no	mel + fas + V → sp + anor + diop
0.48-0.50	no	mel + fas + anor + V → sp + diop
0.51-0.98	no	sp + diop → mel + fas + anor + V
0.99-1.00	no	mel + sp + diop → fas + anor + V
<i>Phases: mel + sp + pv + diop + anor + V</i>		
0.51	yes	sp + diop → mel + pv + anor + V
0-0.28	no	mel + sp + pv + V → anor + diop
0.29-0.47	no	mel + pv + V → sp + anor + diop
0.48-0.50	no	mel + pv + anor + V → sp + diop
0.51-0.99	no	sp + diop → mel + pv + anor + V
1.00	no	mel + sp + diop → pv + anor + V

Table 2c. Same as for Table 2a, Except for Systems Possibly Relevant to the Petrogenesis of Type IV Rims

Phases	Net Reaction *
mel + sp + fas + anor + diop + ol	2.38 sp + 17.03 diop → 1.04 mel + 0.93 fas + 1.75 anor + 3.10 ol
mel + sp + pv + anor + diop + ol	2.36 sp + 16.62 diop → 1.05 mel + 0.10 pv + 1.81 anor + 3.10 ol

* Per mole SiO₂ evolved at rim-external medium contact.

Below, an analysis of net reactions is used to evaluate how the various rim types (Figure 1) may have formed. Phase abbreviations refer to those given in Table 1.

Type I rims. Type I rims principally contain Al-diopside and spinel (Figure 1). Systems possibly relevant for Type I rims include the phases diop (present in rims and possibly in the external medium), ol (in the external medium?), vapor (in the external medium?), sp (in CAIs and rims), mel (in CAIs), and either pv or fas (in CAIs and rims). For systems containing these phases, Table 2a shows that sp and diop are always produced by reaction, and thus sp and diop will always appear in rims. This is true no matter the Mg/[Mg+Si] (= mg) atom ratio in the vapor (Table 2a). Thus it may be possible to form type I rims by reacting melilite + fassaite (or perovskite) ± spinel-bearing CAIs with an external medium that contains vapor ± olivine ± Al-diopside.

Type II rims. Type II rims contain Al-diopside and olivine, but no anorthite (Figure 1). Diop and ol are produced by reaction in systems containing fas (or pv) + mel + sp + vapor, when the vapor has mg = 0.48-0.66 (Table 2a). Therefore it may be possible to form type II rims by reacting melilite + fassaite (or perovskite) ± spinel-bearing CAIs with an external medium that contains vapor ± olivine ± Al-diopside.

Type III rims. These rims contain Al-diopside and anorthite, but no olivine (Figure 1). Diop and anor are produced by reaction in systems that contain fas (or pv) + mel + sp + vapor, when the vapor has mg = 0-0.47 (Table 2b). Thus it may be possible to form type III rims by reacting melilite + fassaite (or perovskite) ± spinel-bearing CAIs with an external medium that contains vapor ± Al-diopside ± anorthite.

Type IV rims. These rims contain layers of spinel, anorthite, Al-diopside, and olivine, in addition to variable amounts of fassaite, perovskite, and melilite (Figure 1). Unlike the other rims described above, at least six major phases are present in these rims or in the adjacent CAIs, suggesting that in a five-component system, these phases alone (without vapor) could have reacted to form the rim assemblage. One possibility is that melilite + spinel + fassaite (or perovskite)-bearing CAIs reacted with olivine or olivine + Al-diopside in the outermost rim layer to form intervening rim layers (Figure 1). However, Table 2c shows that if diffusion was limited to the phases present in these rims and CAIs, then sp and diop would react to form mel, fas or pv, anor, and ol. This would tend to remove spinel and clinopyroxene from the rims unless large amounts of these phases were present in the initial reactants (CAI interior and outer rim layer), for which there is no evidence. Thus closed-system reaction of these phases seems unlikely to account for type IV rims. Instead, it is inferred that for type IV rims, open-system diffusion must have occurred, and another phase not included in the models, possibly vapor, was involved in forming these rims.

Absence of highly refractory phases in rims. An analysis of net reactions can also be used to evaluate why highly refractory phases predicted to be present in rims after a flash heating event, such as refractory glass and CaAl_2O_4 , are always absent. In a system containing both of these phases and fassaite (or perovskite) + melilite + spinel + vapor, refractory glass or CaAl_2O_4 or both are consumed in net reactions for any mg ratio in the vapor [Ruzicka, 1996]. Similarly, for any of the investigated systems that contain either refractory glass or CaAl_2O_4 , but not both, the glass or CaAl_2O_4 tend to be removed by reaction for a wide range in vapor mg ratios [Ruzicka, 1996]. The instability of highly refractory phases in rims is partly due to the assumption of an influx of Si into rims during metasomatism, and partly due to the general absence of phases in CAIs that are richer in Ca and Al than the inferred residues. The combined effect will be to destabilize Si-poor, Ca- and Al-rich phases in rims. Therefore any melilite + fassaite (or perovskite) + spinel-bearing CAIs that were rimmed by refractory glass or Ca-aluminates such as CaAl_2O_4 , CaAl_4O_7 , or $\text{CaAl}_{12}\text{O}_{19}$, would have tended to react with vapor so as to remove the glass and the Ca-aluminate minerals from the rim.

General Constraints for Forming Rim Types I, II, and III

In this section, it is assumed that CAIs containing melilite + spinel + (fassaite or perovskite) react with an external medium containing vapor. The conclusions reached in this section do not depend on specific values of *L* coefficients, but do depend on phase compositions, the assumption that a quasi steady state was

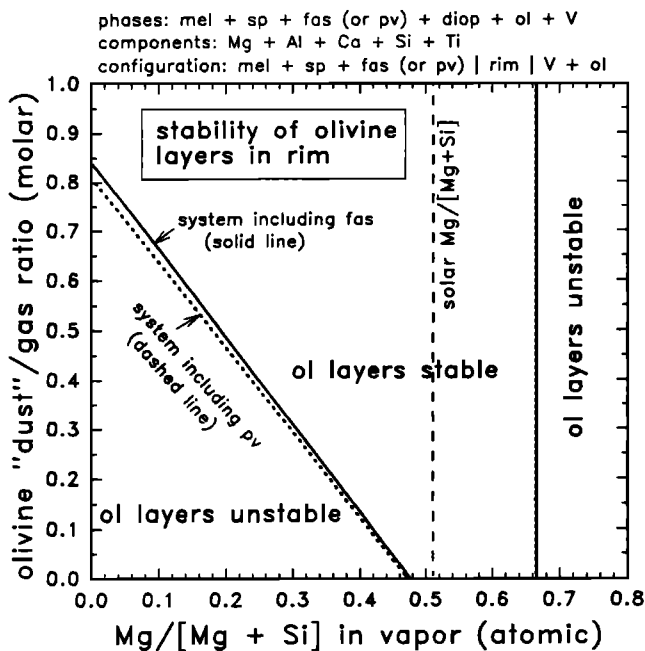


Figure 2. Constraints for olivine-bearing rims. Melilite + spinel + fassaite (or perovskite)-bearing CAIs can react with an external medium that consists of vapor ± olivine to form olivine-bearing layers only if the vapor has an mg (atomic $\text{Mg}/[\text{Mg} + \text{Si}]$) ratio ≤ 0.66 . Olivine-bearing rims will form in the presence of a vapor with $\text{mg} = 0.48\text{-}0.66$, and can form when a vapor with $\text{mg} < 0.48$ is present, provided that the (olivine dust)/gas ratio in the external medium is above a critical value.

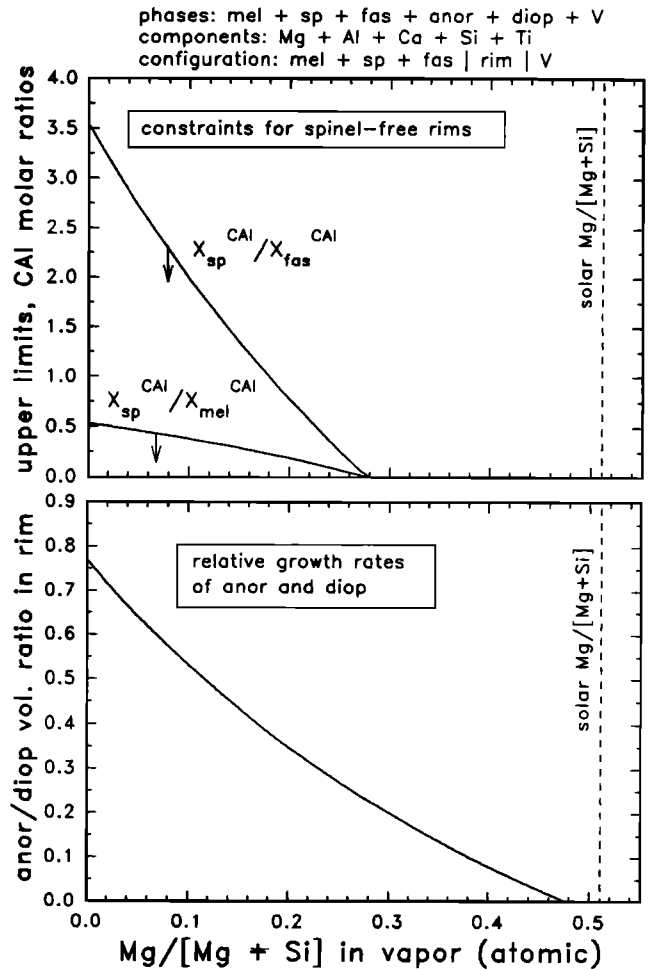


Figure 3. Constraints for rims consisting primarily of clinopyroxene and anorthite. Melilite + spinel + fassaite-bearing CAIs can react with vapor to form anorthite only if the mg (atomic $\text{Mg}/[\text{Mg} + \text{Si}]$) ratio in the vapor is less than 0.48 (bottom diagram). Spinel-free rims can be produced only if the vapor has $\text{mg} \leq 0.28$ and if the spinel/fassaite and spinel/melilite mole fraction ratios ($X_{\text{sp}}^{\text{CAI}}/X_{\text{fas}}^{\text{CAI}}$ and $X_{\text{sp}}^{\text{CAI}}/X_{\text{mel}}^{\text{CAI}}$, respectively) in the CAI interior are below critical values (upper diagram).

reached, and the assumption that closed-system diffusion was occurring.

Figure 2 shows the conditions that are required to form olivine-bearing layers in rims for vapor-bearing systems. To form type II rims, which contain both Al-diopside and olivine, CAIs could have reacted either with (1) pure vapor with intermediate-to-low values of mg ($= 0.48\text{-}0.66$), or with (2) an external medium that was rich both in olivine "dust" and vapor (Figure 2). To form type I rims, which contain Al-diopside but little olivine, CAIs could have reacted with an external medium consisting either of (1) vapor ($\text{mg} < 0.48$) ± olivine, with relatively low abundances of olivine dust, or (2) vapor ($\text{mg} > 0.66$) ± olivine. However, an Mg-rich gas is unlikely to have been involved in rim formation, as such vapor will be produced by net reaction (Table 2a) and would be expected to fill pores or vugs in the layers. As CAI rims (in the three meteorites studied) are notably compact and nonporous, it seems unlikely that gas-filled pores or vugs ever formed in rims. Therefore, type I and II rims can in principle both be explained by the reaction of CAIs with vapor ($\text{Mg}/[\text{Mg} + \text{Si}] \leq$

0.66) ± olivine. In addition, the difference between type I and II rims can be attributed either to the presence of more magnesian gas or a higher proportion of olivine dust in the external medium for type II rims than for type I rims.

Figure 3 shows the conditions that are required to produce spinel-free rims and anorthite-bearing rims for vapor-bearing systems possibly relevant to type III rims. To form anorthite-bearing layers in rims, the vapor must have intermediate-to-low values of mg (≤ 0.48) (Figure 3). For vapor with increasingly lower mg ratios, the anorthite/Al-diopside production ratio in the rims increases (Figure 3). Spinel-free rims in these systems can form only if the gas is relatively Si-rich (mg ≤ 0.28) and if the reacting CAIs are spinel-poor (Figure 3). Thus type III rims could have formed by the reaction of CAIs with a relatively Si-rich gas (Mg/[Mg+Si] ≤ 0.48). Moreover, anorthite-bearing, spinel-free, type III rims could have formed by the reaction of spinel-poor CAIs with an even more Si-rich vapor (Mg/[Mg+Si] ≤ 0.28).

Detailed Comparison of Model and Observed Rim Layers

In this section, a one-to-one comparison is made between model and observed rims in an attempt to model the layer sequences, relative layer widths, and modal compositions of rims. For each model, the observed mode of the relevant CAI interior was used, although the compositions of the external medium are arbitrary. *L* ratios (L_{MgMg}/L_{SiSi} , L_{AlAl}/L_{SiSi} , L_{CaCa}/L_{SiSi} , L_{TiTi}/L_{SiSi}) were varied over a large range (±3 orders of magnitude relative to $L_{ii}/L_{SiSi} = 1$) to see what effects such variations would have on the model rims. The reactants in the external medium were assumed to consist either of vapor alone, vapor + forsterite, or forsterite + Al-diopside.

Table 3 summarizes model-derived constraints for rim analogs based upon comparisons between the model and observed rims. Data for type I, II, III, and IV model rim analogs are given in Tables 3a, 3b, 3c, and 3d, respectively. The layer sequences and layer widths for actual rims are also summarized in these tables.

Schematic diagrams of model layer assemblages corresponding to particular rims are shown in Figures 4a-4g. A variety of features are shown in these diagrams (see the caption to Figure 4

for an explanation). The particular rims that were modeled are representative of those in the Leoville, Vigarano, and Efremovka chondrites [Ruzicka, 1996]. The *L* ratios shown in Figure 4 are representative of those needed to produce layer assemblages that resemble the rims, and the acceptable ranges in *L* ratios to produce the rim sequence analogs are given in Table 3.

Ef-4 (Figure 4a, Table 3a). This "compact" Type A CAI is surrounded by a type I rim consisting of consecutive layers of a granular, melilite-rich zone, a spinel-rich layer containing mainly spinel and fassaite, and a clinopyroxene layer zoned from fassaite to Al-diopside (Table 3a). The melilite-rich zone is fine-grained but has a mode similar to the CAI interior. The spinel-rich and clinopyroxene layers intergrade, and occasional patches of melilite are present between the spinel-rich and clinopyroxene-rich layers. Rare grains of olivine are attached to the outer surface of the clinopyroxene layer.

In the model (Figure 4a), a mel + sp + fas-bearing CAI similar to Ef-4 reacts with an external medium containing 90 mol% vapor (mg = 0.40) and 10 mol% ol. Two layers (mel + sp and sp + diop) and three modally distinct zones (the sp + diop layer is bimodal) are produced (Figure 4a).

The model resembles the observed rim in the overall distribution of phases (mel is concentrated closest to the CAI, followed by sp, followed by diop). Moreover, in the sp + diop zones, μ_{MgO} and μ_{SiO_2} decrease while $\mu_{Al_2O_3}$ and μ_{TiO_2} increase toward the CAI, consistent with the observed zoning of clinopyroxene. The rare grains of olivine found on the outer surface of the CAI could correspond to the small amount of olivine assumed for the external medium. However, the model predicts a lower spinel/clinopyroxene ratio than is observed (Table 3a), and the occasional melilite patches in the rim of Ef-4 are not predicted.

Leo-3 (Figure 4b, Table 3a). Type B CAI Leo-3 is surrounded by a type I rim similar to that around Type A Ef-4 (see above), except that spinel and clinopyroxene do not intergrade, and no granular zone is present immediately beneath the rim (Table 3a).

In the model (Figure 4b), a mel + sp + fas CAI similar in modal composition to Leo-3 reacts with a vapor + ol external medium (same composition as for Ef-4) to produce three layers (sp + fas, sp, and diop).

Table 3a. Model-Derived Constraints for Rims Consisting Primarily of Spinel and Clinopyroxene (Type I Rims)

	Description
Rims	Ef-4: CAI → mel-rich, granular (30-40 μm) → sp-rich (7-35 μm) → cpx + sp ± mel (3-8 μm) → cpx (5-12 μm) → matrix ± ol (3-8 μm)
Model analogs †	Leo-3, Leo-6: CAI → sp-rich (6-150 μm) → ± mel (0-19 μm) → cpx (4-10 μm) → matrix ± ol CAI ± sp ± fas ± mel sp + diop V + ol (Ef-4 analog) CAI ± sp ± fas ± mel sp diop V + ol (Leo-3, Leo-6 analogs)
Vapor composition	mg ~0-0.47
"Dust"/gas ratio	$X_a^{V+ol}/X_v^{V+ol} \leq 0.845$ to 0 for mg = 0 to 0.47, respectively; unconstrained for mg ~0.48-0.66 (Figure 2)
Net reactions	1 mel + 0.49 fas + 1.60 V + 1.35 ol → 0.74 sp + 8.92 diop, mg = 0 1 mel + 0.49 fas + 5.43 V + 0.07 ol → 0.74 sp + 8.92 diop, mg = 0.47
<i>L</i> coefficient ratios	$0.58 \leq L_{MgMg}/L_{SiSi} \leq 2.7$; $0.45 \leq L_{AlAl}/L_{SiSi} \leq 5.3$; $L_{CaCa}/L_{SiSi} \leq 1.5$ (Ef-4 analog) $L_{MgMg}/L_{SiSi} \geq 0.79$; $L_{AlAl}/L_{SiSi} \leq 1.4$; $L_{CaCa}/L_{SiSi} \leq 1.2$ (Leo-3, Leo-6 analogs)
Comments	Ef-4: sp/cpx vol. abundance ratio in rim (~1.7) is higher than predicted (sp/[fas+diop]-0.64); distribution of sp and cpx in Ef-4 rim suggests $L_{CaCa}/L_{SiSi} \sim 0.1-1.5$; model cannot explain mel patches in cpx+sp zone Leo-3, Leo-6: sp/cpx vol. abundance ratio in Leo-3 rim (~0.2) is higher than predicted (sp/[fas+diop]-0.1); model cannot explain discrete mel layer in Leo-6 rim

Phase abbreviations and compositions given in Table 1 and Figure 1; mg, atom fraction Mg/(Mg+Si) in vapor; X_a^b , mole fraction of phase *a* in zone *b*; "±" designation in rim description indicates that phase is locally absent. All model CAIs contain mel + sp + fas. Net reactions are scaled to 1 mole mel consumed.

† Nature of ± sp ± fas ± mel zone adjacent to CAI depends on the mode of the CAI as follows. When $X_{mel}^{CAI}/X_{fas}^{CAI} < 2.04$, the zone consists of sp + fas; when $X_{mel}^{CAI}/X_{fas}^{CAI} > 2.04$, the zone consists of sp + mel; when $X_{mel}^{CAI}/X_{fas}^{CAI} = 2.04$, the zone is absent.

Table 3b. Model-Derived Constraints for Rims Consisting Primarily of Spinel, Clinopyroxene, and Olivine (Type II Rims)

	Description
Rims	Leo-1: CAI → sp-rich (10-35 μm) → cpx + sp (8 μm) → cpx + ol (7-8 μm) → ol-rich (≤40-50 μm) → matrix Leo-16, Leo-17: CAI → sp-rich (0-25 μm) → ± mel (0-5 μm) → cpx (5-17 μm) → ol-rich (0-30 μm) → matrix
Model analogs †	CAI ± sp ± fas ± mel sp + diop diop + ol V + ol (Leo-1 analog) CAI ± sp ± fas ± mel sp diop V + ol (Leo-16, Leo-17 analogs)
Vapor composition	mg ~0-0.66
"Dust"/gas ratio	$X_{ol}^{v+ol}/X_v^{v+ol} > 0.845$ to 0 for mg = 0 to 0.47, respectively; unconstrained for mg -0.48-0.66 (Figure 2)
Net reactions	1 mel + 0.49 fas + 1.60 V + 1.35 ol → 0.74 sp + 8.92 diop, mg = 0 1 mel + 0.49 fas + 5.73 V → 0.74 sp + 8.92 diop + 0.03 ol, mg = 0.48 1 mel + 0.49 fas + 160.33 V → 0.74 sp + 8.92 diop + 51.56 ol, mg = 0.66
L coefficient ratios	$0.03 \leq L_{MgMg}/L_{SiSi} \leq 2.7$; $0.45 \leq L_{AlAl}/L_{SiSi} \leq 5.3$ (Leo-1 analog) $0.68 \leq L_{MgMg}/L_{SiSi} \leq 1.15$; $0.89 \leq L_{AlAl}/L_{SiSi} \leq 1.5$; $L_{CrCr}/L_{SiSi} \leq 2.3$ (Leo-16, Leo-17 analogs)
Comments	Leo-1: sp/cpx vol. abundance ratio in rim (~1.4) is higher than predicted (sp/[fas+diop]~0.1) Leo-16, Leo-17: sp/cpx vol. abundance ratio in Leo-17 rim (~0.5) is higher than predicted (sp/[fas+diop]~0.26); model cannot explain discrete mel layer in Leo-16 rim

Nomenclature and format same as for Table 3a.

† Nature of ± sp ± fas ± mel zone same as in Table 3a.

The predicted spatial distribution of phases (sp closer to the CAI, diop further away), and the variations of μ_{MgO} , μ_{SiO_2} , $\mu_{AlO_3/2}$, and μ_{TiO_2} in the diop layer, are consistent with the observed rim texture and with chemical variations in clinopyroxene. The model predicts that a very thin sp + fas layer (comprising only 0.7% of the total layer thickness) will form adjacent to the CAI interior, and no such layer is evident in the rim of Leo-3. Another discrepancy between the model and observed rims is that the spinel/clinopyroxene ratio in the rim of Leo-3 is higher than predicted (Table 3a). Finally, some type I rims similar to Leo-3 contain a discrete layer of melilite between the inner spinel and outer clinopyroxene layers (Table 3a), and such a melilite layer is not predicted by the models.

Leo-1 (Figure 4c, Table 3b). The type II rim surrounding this Type B1 CAI consists of an inner spinel-rich layer, followed by a clinopyroxene layer (zoned from fassaite to Al-diopside away from the CAI), followed by an olivine-rich layer. Each of the layers intergrade. The olivine-rich layer partly consists of individual grain clumps (Table 3b).

In the model (Figure 4c), a mel + sp + fas CAI similar in modal composition to the outer portion ("mantle") of Leo-1 reacts with an external medium containing 50 mol% vapor (mg = 0.40) and 50 mol% ol to form three layers (mel + sp, sp + diop, diop

+ ol) and four modally distinct zones (the sp + diop layer is bimodal). The vapor + ol external medium assumed in the model may correlate with the clumpy, outermost portion of the olivine-rich layer, which appears to have formed by the accumulation of olivine grains onto the surface of the CAI [Ruzicka and Boynton, 1993; Ruzicka, 1996].

The model resembles the observed rim in the overall spatial distribution of spinel, clinopyroxene, and olivine (spinel closest, olivine furthest from the CAI), and in the gradation of spinel with clinopyroxene, and of clinopyroxene with olivine. Furthermore, predicted variations in μ_{MgO} , μ_{SiO_2} , $\mu_{AlO_3/2}$, and μ_{TiO_2} in the sp + diop layer are consistent with observed zoning patterns in clinopyroxene. The model predicts that a discrete mel + sp layer, with a mode very similar to the CAI interior, will form adjacent to the CAI interior (Figure 4c). No such layer is obvious around Leo-1. Once again, the model underestimates the spinel/clinopyroxene ratio of the rim (Table 3b).

Leo-17 (Figure 4d, Table 3b). This Type B CAI is surrounded by a type II rim consisting of consecutive spinel-rich, clinopyroxene, and olivine layers (Table 3b). The olivine layer is notably compact.

In the model (Figure 4d), a CAI with a mode similar to Leo-17 reacts with an external medium containing 25 mol% vapor (mg

Table 3c. Model-Derived Constraints for Rims Consisting Primarily of Clinopyroxene and Anorthite, With or Without Spinel (Type III Rims)

	Description
Rims	Vig-9, Vig-10: mel → anor (0-13 μm) → cpx (1-30 μm) → matrix Vig-11, Leo-11: CAI → anor-rich (0-20 μm) → cpx (9-20 μm) → matrix ± ol ± cpx (6 μm) → matrix
Model analogs †	CAI mel + fas ± mel ± fas anor diop V (Vig-9, Vig-10 analogs) CAI sp ± fas ± mel sp anor diop V (Vig-11, Leo-11 analogs)
Vapor composition	mg ~0-0.27 (Vig-9, Vig-10 analogs) mg ~0.28-0.47 (Vig-11, Leo-11 analogs)
CAI mode	X_{sp}^{CAI} required to be low for Vig-9, Vig-10 analogs (Figure 3)
Net reactions	1 mel + 0.53 sp + 0.15 fas + 2.91 V → 1.39 anor + 2.74 diop, mg = 0 1 mel + 0.02 sp + 0.29 fas + 4.01 V → 0.83 anor + 5.23 diop, mg = 0.27 1 mel + 0.48 fas + 5.56 V → 0.70 sp + 0.04 anor + 8.73 diop, mg = 0.47
L coefficient ratios	$L_{AlAl}/L_{SiSi} \geq 0.11$ (Vig-9, Vig-10 analogs, at low mg only) $L_{CrCr}/L_{SiSi} \leq 1.3$ (Vig-11, Leo-11 analogs, at high mg only)
Comments	Vig-9, Vig-10: model predicts anor/diop vol. abundance ratios of ~0.24-0.78 Vig-11, Leo-11: model predicts anor/diop vol. abundance ratios of ~0-0.78; in contrast to model predictions, sp and anor do not always form distinct layers

Nomenclature and format same as for Table 3a.

† Nature of the two zones, ± mel ± fas (monomineralic mel or fas, if present) and sp ± fas ± mel (sp + fas or sp + mel, if present), depends on the mode of the CAI.

Table 3d. Model-Derived Constraints for Rims Containing Spinel, Anorthite, Clinopyroxene, and Olivine (Type IV Rims)

	Description
Rims	Vig-1, Vig-3, Vig-16: CAI → sp-rich (0-40 μm) → anor/mel (0-10 μm) → cpx (2-7 μm) → ol-rich (1-50 μm) → matrix
Model analogs †	CAI sp ± fas ± mel sp anor diop ol + diop
Open-system flux ‡	$J_{\text{CaO}}^{\text{net}} \geq 2.5$
Net reactions	1 mel + 0.22 fas + 0.82 ol → 0.79 sp + 0.03 anor + 4.07 diop + 1.06 CaO (for $J_{\text{CaO}}^{\text{net}} = 4$ and $L_{\text{il}}/L_{\text{Bisi}} = 1$ except for $L_{\text{MgMg}}/L_{\text{Bisi}} = 1.65$) 1 mel + 0.02 fas + 0.17 ol → 0.35 sp + 0.54 anor + 0.41 diop + 1.37 CaO (for $J_{\text{CaO}}^{\text{net}} = 8$ and $L_{\text{il}}/L_{\text{Bisi}} = 1$ except for $L_{\text{CaCa}}/L_{\text{Bisi}} = 2$)
L coefficient ratios	$0.25 \leq L_{\text{MgMg}}/L_{\text{Bisi}} \leq 1.7$; $0.03 \leq L_{\text{AlAl}}/L_{\text{Bisi}} \leq 5.2$; $0.74 \leq L_{\text{CaCa}}/L_{\text{Bisi}} \leq 2.5$, for $J_{\text{CaO}}^{\text{net}} \sim 3-10$
Comments	model cannot explain local presence of monomineralic mel or bimineralic mel + anor layers in the rims of Vig-1 and Vig-3; sp/cpx vol. ratios in the rims of Vig-1, Vig-3, and Vig-16 (~1-3) are similar to or higher than sp/(fas+diop) ratios in model rims (~0.85-2.1); model predicts rim anor/diop vol. ratios of ~0-2

Nomenclature and format same as for Table 3a. Calculations assume a CAI mode ($X_{\text{mel}}^{\text{CAI}} = 0.58$, $X_{\text{sp}}^{\text{CAI}} = 0.40$, $X_{\text{fas}}^{\text{CAI}} = 0.02$) representative of Vig-1, Vig-3, and Vig-16 and a mode for the ol + diop reactant ($X_{\text{ol}}^{\text{ol+diop}} = 0.90$) representative of the olivine-rich layer in the rims.

† Nature of sp ± fas ± mel zone (bimineralic and spinel-bearing if present) depends on the mode of the CAI and the value for the open-system flux.

‡ $J_{\text{CaO}}^{\text{net}}$ is the moles of CaO diffusing out of the layer assemblage at the diop - (ol+diop) contact per unit area per unit time, normalized to the number of moles of SiO₂ evolved per unit time at the same contact.

= 0.40) and 75 mol% ol to produce four layers (mel + sp, sp, diop, ol).

The spatial distribution of these phases (sp closest, ol furthest away from the CAI) in the model resemble that in the rim, and the predicted variations in μ_i for $i = \text{MgO}$, $\text{AlO}_{3/2}$, SiO_2 and TiO_2 in the diop layer are consistent with the observed zoning of the clinopyroxene layer. The model predicts that a very thin mel + sp layer (0.5% of the total layer thickness) will form adjacent to the CAI interior (Figure 4d), and no such layer is obvious in the rim. As with other rims, the spinel/clinopyroxene ratio in the rim of Leo-17 is higher than predicted (Table 3b). Finally, other CAIs have rims that resemble Leo-17, except that in these CAIs a melilite layer, which is not predicted by the models, intervenes between the spinel-rich and clinopyroxene layers (Table 3b).

Vig-9 and Vig-10 (Figure 4e, Table 3c). Vig-9 and Vig-10 are melilite-rich fragments that have incomplete type III rims consisting of consecutive layers of anorthite and Al-diopside (Table 3c). Al-diopside is zoned with Si and Mg decreasing and Al increasing toward the melilite, while Ti is relatively constant. Isolated grains of fassaite, but no spinel, are contained in their interiors, and no spinel or olivine is present in either rim.

In the model (Figure 4e), a CAI that contains small proportions of sp and fas (2 vol% each) reacts with a Si-rich vapor ($\text{mg} = 0.10$) to form four layers (mel + fas, mel, anor, diop). The spatial distribution of these phases in the model rim resembles that of the Vig-9 and -10 rims (melilite-rich CAI interiors, followed by consecutive layers of anorthite and Al-diopside). The model predicts that mel + fas and mel layers, composed mainly or entirely of mel, will form between the anor layer and the CAI interior (Figure 4e), and no such discrete layers are observed around Vig-9 or -10. The predicted variation of μ_{SiO_2} and $\mu_{\text{AlO}_{3/2}}$ in the diop layer is consistent with the observed zoning in the clinopyroxene layer, but in the model, μ_{MgO} decreases away from the CAI (Figure 4e), while in the clinopyroxene layer, the concentration of MgO increases away from the CAI. This discrepancy can be explained if MgO was not an independently diffusing component (that is, the concentration of MgO may have been determined by the concentration of SiO₂ or Al₂O₃).

Vig-11 (Figure 4f, Table 3c). Type B CAI Vig-11 contains type III rims of consecutive anorthite- and clinopyroxene-rich layers that surround both the exterior of the object and several "pores" within the object. The "internal" and "external" rims differ

slightly. In the external rim, an inner layer composed roughly of equal proportions of spinel and anorthite with accessory fassaite is followed by a layer of clinopyroxene, whereas in the internal rims, anorthite often forms a discrete layer between the clinopyroxene layer and a poorly defined inner zone of spinel + fassaite (Table 3c). The anorthite layer is locally absent in the internal rims.

In the model (Figure 4f), a CAI with a modal composition similar to Vig-11 reacts with a relatively Si-rich vapor ($\text{mg} = 0.30$) to form four layers (sp + fas, sp, anor, and diop). The spatial distribution of these phases in the model resemble that observed for the rims, especially for the internal rims (with spinel concentrated closest to the CAI, followed by anorthite, followed by Al-diopside). Moreover, the predicted variations in μ_i for $i = \text{MgO}$, $\text{AlO}_{3/2}$, SiO_2 and TiO_2 in the diop layer are consistent with the observed zoning of the clinopyroxene layers. However, in the external rim, spinel and anorthite are intergrown and do not form separate layers, in contrast to the models.

Vig-1, Vig-3, Vig-16 (Figure 4g, Table 3d). Vig-1, -3, and -16 are compact Type A CAIs surrounded by type IV rims consisting of four consecutive rim layers: an inner spinel-rich layer, a monomineralic layer of anorthite or melilite (or a bimineralic layer of anorthite + melilite), a clinopyroxene layer, and finally an olivine-rich layer that is notably compact (Table 3d).

In the model (Figure 4g), a CAI with a modal composition representative of these CAIs reacts with an external medium consisting of 90 mol% ol and 10 mol% diop, during open-system diffusion. The mode of the ol + diop "external medium" was chosen so as to resemble the compact, olivine-rich layer. In the model, four layers are produced (mel + sp, sp, anor, and diop) between the CAI interior and the ol + diop zone (Figure 4g). An open-system loss of CaO at the diop - (ol + diop) contact is required to stabilize the diop layer in the rim (Table 3d).

The spatial distribution of these phases in the model resembles that in the observed rims, and the predicted variations in μ_i for $i = \text{MgO}$, $\text{AlO}_{3/2}$, SiO_2 , and TiO_2 in the diop layer are consistent with the observed zoning of the clinopyroxene rim layer. The model predicts the formation of an innermost, mel + sp layer that has a mode similar to that of the CAI interior (Figure 4g), but no such layer is apparent in the rim. The model fails to account for the local presence of melilite in either monomineralic mel or bimineralic anor + mel layers between the spinel-rich and

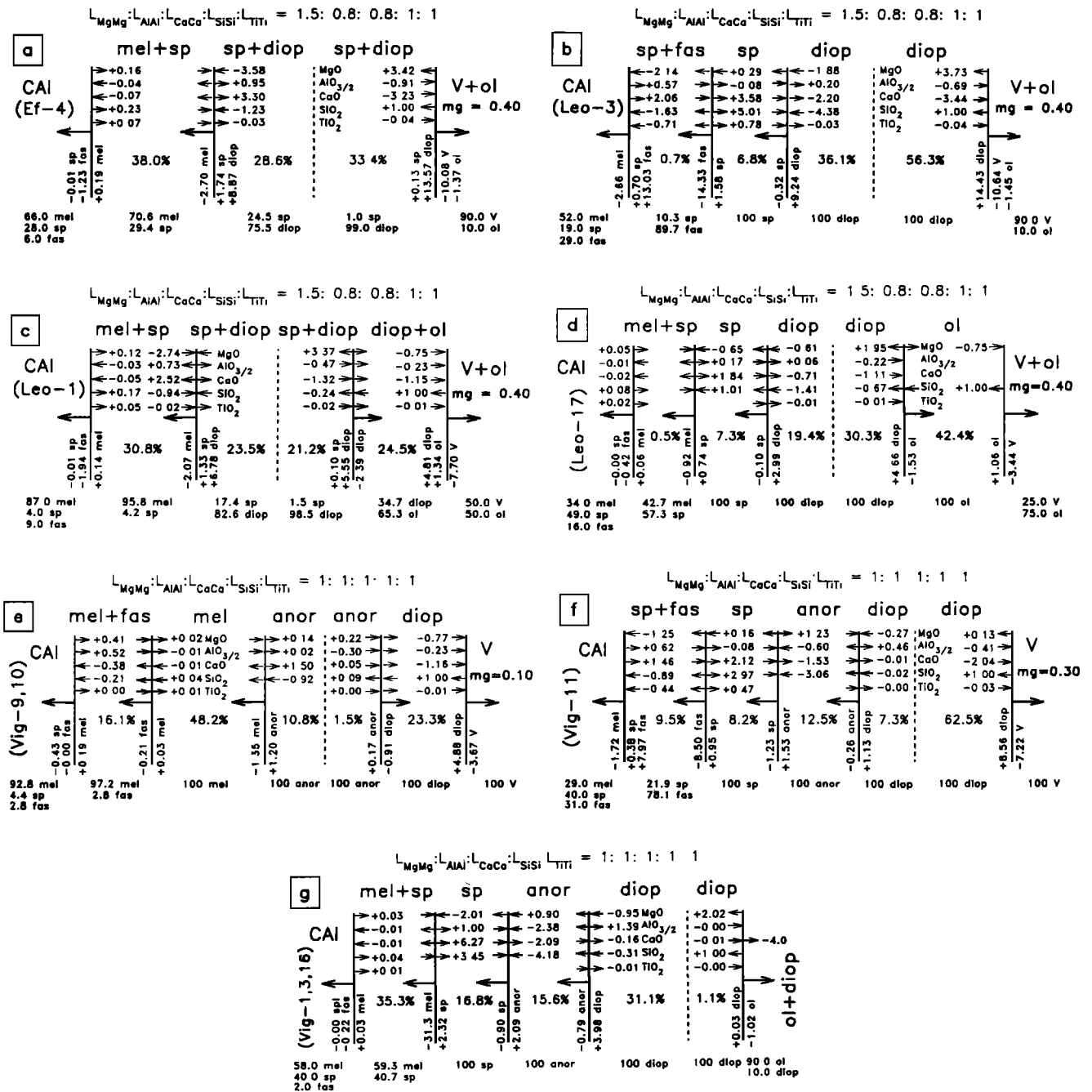


Figure 4. Schematic illustration of model results for CAI rim analogs. (a-b) Rims that consist primarily of spinel and clinopyroxene (type I); (c-d) rims that consist primarily of spinel, clinopyroxene, and olivine (type II); (e-f) rims that consist primarily of clinopyroxene and anorthite, with or without spinel (type III); (g) rims that contain spinel, anorthite, clinopyroxene, and olivine (type IV). In each diagram the CAI is at left, and the external medium is at right. Solid vertical lines represent layer contacts, which move in the direction indicated by the heavy arrows. The dashed line represents a stationary inert marker that bisects one of the layers into two zones. Mineral zones are designated by the phases they contain (see Table 1 for phase abbreviations and compositions). The prominent numbers near the centers of the zones give zone widths in percent total rim thickness, and layer modes are given below the zones in mol%. Reaction coefficients (in mol/unit-time) for phases and components at each layer contact are scaled to the evolution of 1 mol SiO_2 per unit time at the rim-external medium contact, with "plus sign" and "minus sign" designations referring to components that are locally evolved and consumed, respectively. Small arrows give the direction components are diffusing (to lower values of chemical potential). For example, in Figure 4a (Ef-4 rim analog), at the contact between sp+diop and V+ol, the local reaction can be described as $10.08 \text{ vapor} (mg = 0.40) + 1.37 \text{ ol} + 0.91 \text{ } AlO_{3/2}$ (diffusing from the CAI) + 3.23 CaO (from the CAI) + $0.04 \text{ } TiO_2$ (from the CAI) \rightarrow $0.13 \text{ sp} + 13.57 \text{ diop} + 3.42 \text{ MgO}$ (from V+ol) + $1.00 \text{ } SiO_2$ (from V+ol). In the same sequence, the local reaction at the contact between the mel+sp and sp+diop zones can be described as $2.70 \text{ mel} + 3.58 \text{ MgO}$ (diffusing from the CAI and V+ol) + $1.23 \text{ } SiO_2$ (from the CAI and V+ol) + $0.03 \text{ } TiO_2$ (from the CAI) \rightarrow $1.74 \text{ sp} + 8.87 \text{ diop} + 0.95 \text{ } AlO_{3/2}$ (toward the CAI and V+ol) + 3.30 CaO (toward the CAI and V+ol).

clinopyroxene layers (Table 3d). Finally, as with other rims, the model tends to underestimate the spinel/clinopyroxene ratio in the layer assemblage (Table 3d).

Summary. Several conclusions can be drawn from detailed comparisons between model and observed rims. Most important, the overall mineral zoning structure and textures of rims can be explained by a quantitative model in which most of the layers form by metasomatism. Moreover, the models make predictions regarding chemical potential variations that are consistent with the observed major-element zoning of clinopyroxene in rims. This suggests that CAI rim layers formed primarily by metasomatism.

Some discrepancies between model and observed rims suggest that the metasomatism model, while generally valid, is oversimplified. The main discrepancies are that (1) melilite layers or patches between spinel-rich and clinopyroxene layers cannot be produced by metasomatism, and (2) the models consistently underestimate the spinel/clinopyroxene ratios of rims (by factors of ≈ 2 -40).

The presence of melilite layers or patches between spinel-rich and clinopyroxene layers in rims is probably attributable to a failure in achieving a complete quasi steady state condition during layer formation, either because pressure or temperature were changing too rapidly, or because the composition of the initial reactants did not remain constant with time. In the models, melilite is disappearing by reaction, and incomplete removal of melilite from within the layer assemblages could account for the presence of such melilite.

The consistently elevated spinel-to-clinopyroxene ratio in rims compared to models also can be explained if a quasi steady state was not completely achieved. In particular, some of the spinel in rims probably was produced by processes other than metasomatism. It has been experimentally demonstrated that spinel can form on the surfaces of CAI melt droplets by a nucleation effect [Beckett and Grossman, 1982; Paque and Stolper, 1983; Murrell and Burnett, 1986], and this effect could account for the apparent surplus of spinel in rims. Alternatively, if rims formed initially through the partial vaporization of CAIs during a flash heating episode, then spinel could have accumulated as an unmelted phase at the residue-CAI interior interface through partial melting of the CAI interiors, accompanying a flash heating event [Murrell and Burnett, 1987]. If "excess" spinel formed in this way, it would require that the spinel-rich layer in rims formed approximately at the innermost extent of partial melting of the CAIs during a vaporization event. In any case, if a steady state had been achieved during layer growth, then any "excess" spinel in the vicinity of rims would have been consumed until the proportion predicted by the models was obtained.

It seems likely that at least some of the spinel in rims formed by metasomatism, as an inner spinel-rich layer is predicted to form by the reaction of melilite-bearing CAIs with plausible (Si- and Mg-rich) external environments. If all of the layer-forming clinopyroxene formed by metasomatism, roughly 3-50% of the spinel in rims can be attributed to metasomatic growth.

The models also predict the presence of one or more additional layers between the spinel-rich layer and the CAI interior which are usually not observed. However, such layers are either very thin or have modes similar to the CAI interior. Melilite-rich layers of similar modal composition to the interiors of the CAIs probably would not be recognized as distinct layers, unless (as in Ef-4) the layers were texturally different from the interiors. Very thin layers (e.g., Leo-3, Figure 4b; and Leo-17, Figure 4d) would be difficult to recognize, and may have been

incapable of forming, if the scale of local equilibrium were larger than the predicted layer itself.

Timescales of Metasomatism Inferred From Isotopic Exchange

The timescale of CAI metasomatism can be constrained from certain radial variations in Mg isotopic composition within CAIs, which probably reflect Mg isotopic exchange between the CAIs and an external medium during the same metasomatic event that produced the mineral layers. Pertinent experimental data are available for isotopic exchange in melilite [Morioka and Nagasawa, 1991], the principal constituent of coarse-grained CAIs, and for CAI-like melts [Sheng et al., 1992]. The timescale for layer formation could be more directly determined if absolute values of L coefficients and absolute changes in chemical potentials (μ_i) across mineral zones or the layer assemblage were known [Ruzicka, 1996], but for rims these parameters are either poorly known or model-dependent.

Several CAIs have radial Mg-isotope profiles that are characterized by near-normal $^{25}\text{Mg}/^{24}\text{Mg}$ ratios (or F_{Mg} values) near their margins and enrichments within their interiors. The best-defined F_{Mg} gradient of this type is probably that of CAI E2, a 2-cm-diameter, melilite-rich (Type A) CAI in Efremovka [Fahey et al., 1985, 1987; Goswami et al., 1994] (Figure 5).

Mg-isotope profiles of this type are opposite to the sense expected for the vaporization of CAI margins, and are better explained as a result of Mg isotopic exchange between the CAIs and an external medium with near-normal Mg isotope

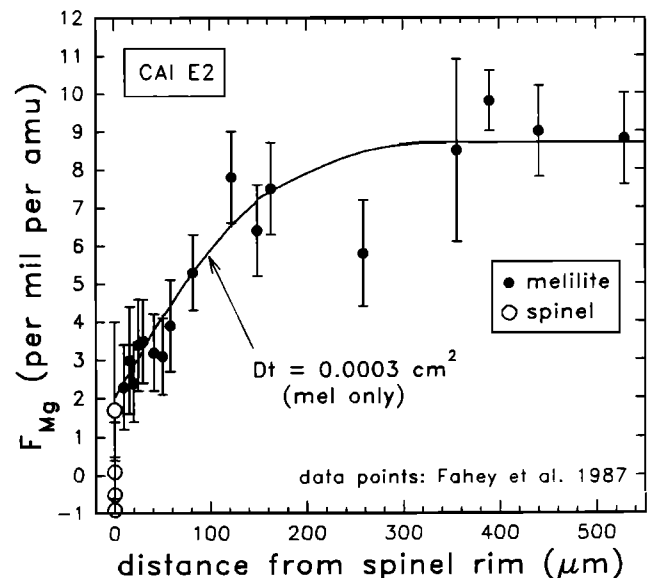


Figure 5. Radial gradient of Mg isotopic composition in melilite from Type A CAI E2 [Fahey et al., 1987] compared to a diffusion profile. $F_{\text{Mg}} = \{[(^{25}\text{Mg}/^{24}\text{Mg})_{\text{unknown}} - (^{25}\text{Mg}/^{24}\text{Mg})_{\text{standard}}] \cdot 1000\}$, where $F_{\text{Mg}} = 0$ for "normal" (i.e., terrestrial standard) compositions. The diffusion profile shown is a best fit to the melilite data using the equation $F_{\text{Mg}} = A + B \cdot \text{erf}(Cd)$ [Fahey et al., 1987], where d is the distance from the spinel rim (in centimeters), $C = 1/(Dt)^{0.5} = 57.735 \text{ cm}^{-1}$ (or $Dt = 0.0003 \text{ cm}^2$), $A = 2.0$ (F_{Mg} at $d = 0$), and $B = 6.7$. The reasonably good match between the measured and calculated profiles implies that the outermost $\approx 350 \mu\text{m}$ of the CAI diffusively exchanged Mg isotopes with the external environment surrounding the CAI.

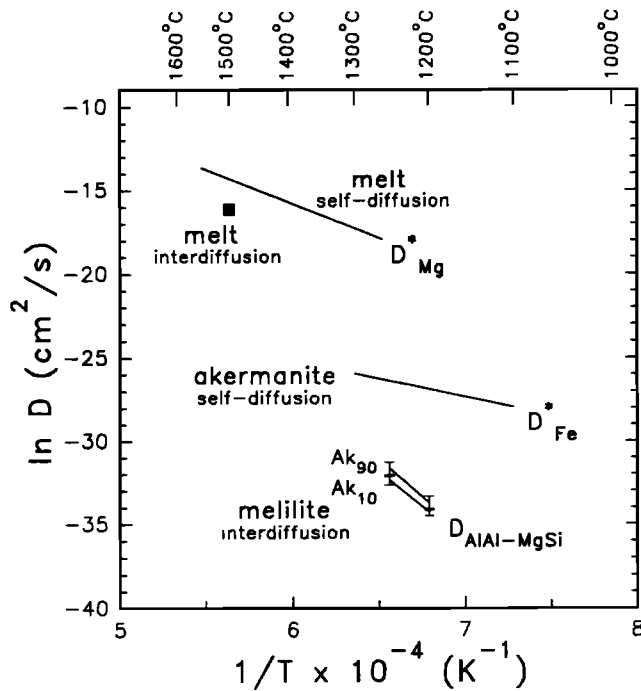


Figure 6. Summary of selected diffusion data relevant to CAI petrogenesis. D_{Mg}^* (melt) is the self-diffusion rate of Mg in POI melts [Sheng *et al.*, 1992], D_{Fe}^* (akermanite) is the tracer diffusion rate of Fe^{2+} in akermanite parallel to the *c* axis [Morioka and Nagasawa, 1991], and $D_{\text{AlAl-MgSi}}$ (melilite) is the interdiffusion rate in Ak_{10-90} melilite [Morioka and Nagasawa, 1991]. The solid symbol represents a typical value for interdiffusion in silicate melts [Kress and Ghiorso, 1993]. D_{Fe}^* (akermanite) is representative of the isotopic diffusion rate in melilite for small, divalent cations [Morioka and Nagasawa, 1991], while D_{Mg}^* (melt) is representative of the chemical and isotopic diffusion rate in a CAI melt.

composition [Goswami *et al.*, 1994]. A less likely alternative is that such radial gradients formed by the condensation of material onto CAIs from a reservoir that was changing isotopic composition with time [Fahey *et al.*, 1987]. However, the F_{Mg} gradient in E2 has the form of an error function (i.e., a diffusion profile) [Fahey *et al.*, 1985, 1987] (Figure 5), and there is no a priori reason why this should be the case for a condensation mechanism. The condensation hypothesis is further weakened by the lack of any textural or mineralogical discontinuities associated with the F_{Mg} profile, as such discontinuities would be expected for a gas that was changing composition with time. Thus diffusive isotopic exchange is considered to be a better explanation for the Mg isotope gradient in E2, and for similar Mg-isotope variations in other CAIs [Lorin *et al.*, 1978; MacPherson *et al.*, 1986; Davis *et al.*, 1987].

The Mg-isotope profile in E2 melilite (Figure 5) can be used in conjunction with experimental data (Figure 6) to constrain the thermal event associated with metasomatism, provided that the form of the profile was constrained only by diffusion within the CAI and not by other factors. A best fit to the melilite profile suggests $Dt = 0.0003 \pm 0.0001 \text{ cm}^2$, where D is the relevant diffusion coefficient and t is time (Figure 5).

Very different timescales are implied depending on whether isotopic diffusion occurred in melilite or in melt (Figure 6). For example, at a temperature of 1250°C, $\ln D \approx -18 \text{ cm}^2/\text{s}$ for Mg self-diffusion in melt (which should be appropriate to Mg isotopic

diffusion in melt), and $\ln D \approx -26 \text{ cm}^2/\text{s}$ for Fe^{2+} tracer diffusion in akermanite (which should be similar to Mg^{2+} isotopic diffusion in melilite) (Figure 6). This implies that the F_{Mg} profile in E2 would have formed in melt in ≈ 5.5 hours and in melilite in ≈ 1.9 years for isothermal diffusion at 1250°C. By comparison, AlAl-SiMg interdiffusion in melilite is a slow process, with $\ln D \approx -32 \text{ cm}^2/\text{s}$ at 1250°C (Figure 6). Thus, for the timescales necessary to produce the Mg isotopic variation at 1250°C, major-element zoning in melilite would have been restricted to $\approx 0.16 \mu\text{m}$ or $\approx 9 \mu\text{m}$, depending on whether the Mg-isotope profile was initially established in melt or in melilite, respectively.

An estimate of the cooling rate can be obtained if it is assumed that Mg exchange in E2 occurred during cooling. The interiors of Type B CAIs appear to have been heated to subliquidus temperatures of ≈ 1400 - 1450°C , based on a comparison of the textures in natural and synthetic CAIs [Stolper and Paque, 1986]. If the same maximum temperatures were pertinent for Mg-isotope exchange in E2, initial cooling rates of ≈ 0.1 - $2^\circ\text{C}/\text{h}$ and ≈ 2000 - $5000^\circ\text{C}/\text{h}$ are estimated for Mg isotopic diffusion in akermanite and melt, respectively, assuming an "asymptotic" cooling model [Ganguly *et al.*, 1994] (Figure 7). These cooling rates would be lower limits if diffusion occurred at higher temperatures and upper limits if diffusion was initiated at lower temperatures. Although the cooling rates for isotopic diffusion in melilite (≈ 0.1 - $2^\circ\text{C}/\text{h}$ at ≈ 1400 - 1450°C) partly overlap those inferred from textures and major element zoning patterns in Type B CAIs (≈ 1 - $50^\circ\text{C}/\text{h}$) [MacPherson *et al.*, 1984; Stolper and Paque, 1986], the cooling rates based on isotopic diffusion in melt are so rapid as

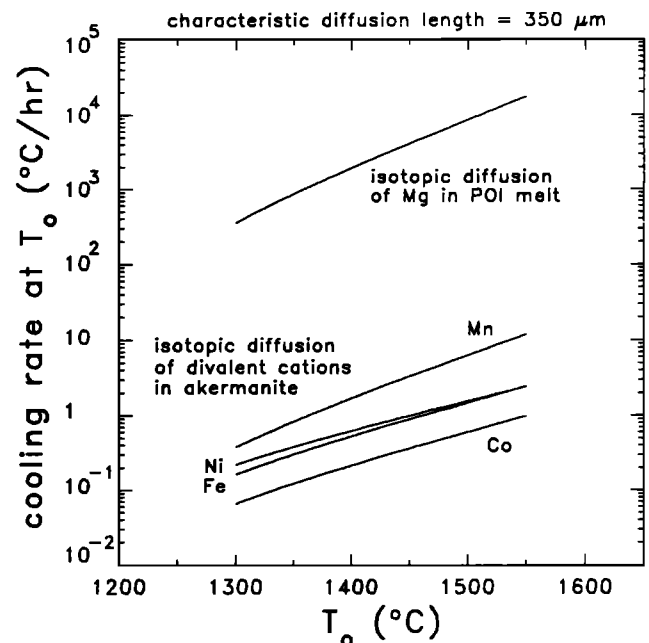


Figure 7. Calculated cooling rates near liquidus and subliquidus temperatures for CAIs necessary to result in a characteristic diffusion length of $350 \mu\text{m}$, the same length as inferred for Mg isotopes in CAI E2 (Figure 5). An asymptotic cooling model [Ganguly *et al.*, 1994] was assumed. T_0 is the maximum temperature at the onset of diffusion during cooling. Diffusion data were taken from Sheng *et al.* [1992] for Mg self diffusion in POI melt, and from Morioka and Nagasawa [1991] for tracer diffusion of divalent cations in akermanite (Figure 6). Calculations assume that diffusion was limited only by diffusion within the CAIs, which is probably an invalid assumption for melt (see text and Figure 8).

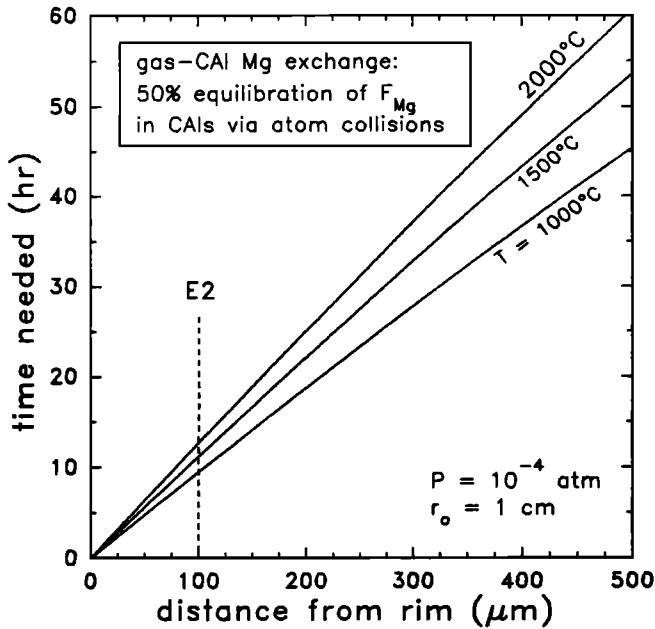


Figure 8. Conditions for which Mg isotopic exchange between a CAI and surrounding gas will be limited by the number of gas molecule collisions with the CAI surface. The curves show the time needed to change the Mg isotopic composition of a 1-cm-radius spherical CAI by 50% to a given depth in the CAI, assuming a gas of solar composition [Anders and Grevesse, 1989] at 10^{-4} atm pressure and at three different temperatures, an average Mg content in a coarse-grained CAI [Ruzicka, 1996], and infinitely rapid diffusion. The depth corresponding to a 50% change in F_{Mg} for CAI E2 (Figure 5) is indicated. This figure shows that if E2 exchanged Mg isotopes with a low-pressure gas, then diffusion would be limited by the number of collisions on the surface of the CAI for a heating event that was less than ≈ 10 hours in duration.

to be suspect. Rapid isotopic equilibration in CAI melts would preclude the formation of the observed Mg isotope profiles, as the CAIs would be expected to attain nearly uniform Mg isotopic compositions throughout their interiors.

However, isotopic diffusion may still have occurred within melt and not been limited by the rate of diffusion in the melt, if the availability of Mg atoms in the external medium were the limiting factor. Such a circumstance could arise if the external medium consisted of a low-pressure gas. This situation is illustrated in Figure 8, which shows the time needed to change the F_{Mg} value in a 1-cm-radius CAI by 50% to a certain depth within the CAI. The calculation in Figure 8 is based upon the expected collision rate of Mg atoms with the CAI surface, which depends only on the pressure and temperature of the gas, the surface area of the CAI, and the Mg content in the gas and CAI. For CAI E2, the F_{Mg} profile changes by 50% at a depth of ≈ 100 μm (Figure 5), and from Figure 8 this corresponds to a time of ≈ 10 hours for exchange with a gas at a pressure of 10^{-4} bars and a temperature of ≈ 1000 - 2000°C . Thus, for a heating event less than 10 hours in duration, the limiting factor for isotopic exchange between a CAI such as E2 and the surrounding gas would not be the diffusion rate in the CAI, but the number of atom collisions on the CAI surface. In this case, cooling rate estimates based on the assumption that diffusion was the rate-limiting step (Figure 7) would be invalid for melt, but not for melilite.

To summarize, the Mg isotope profile in CAI E2 can be explained in one of two ways. Isotopic exchange could have occurred at high ($>$ solidus and possibly $>$ liquidus) temperatures, with isotopic diffusion occurring primarily through melt out of which melilite crystallized, if the CAI were exchanging Mg isotopes with a low-pressure gas during a short (< 10 hour) duration heating episode. Alternatively, isotopic exchange could have occurred at low ($<$ liquidus) temperatures, with diffusion occurring primarily through melilite. In the latter case, the initial cooling rate would have been ≈ 0.1 - $2^\circ\text{C}/\text{h}$ at a temperature of ≈ 1400 - 1450°C .

Implications for Nebular Processes and Environments

Although the modes of CAIs vary from object to object, there is no obvious correlation between these modes and rim type. Moreover, similar L coefficient ratios can account for different layer structures around different CAIs (Table 3). This suggests that the primary control in rim structure was the composition of the external medium. Model results suggest that vapor was an important constituent during CAI rim metasomatism. An Mg-Si-bearing vapor (with or without a coating of olivine on CAIs) could have reacted with CAIs to form rim types I, II, and III. For rim type IV, vapor could have coexisted with olivine + clinopyroxene in the external medium, and such vapor could have served as a sink for Ca diffusing out of the CAIs and rims. The apparently widespread occurrence of vapor during rim metasomatism is consistent with a "nebular" setting for rim formation, although metasomatism could have occurred in any gas-rich environment.

Nonuniform conditions in the external medium appear to have been primarily responsible for producing the variety of rim types. All of the rims could have formed by the reaction of CAIs with a nonsolar, Si-rich gas ($mg < 0.28$), but if so, olivine/gas ratios in the external medium are required to have been different for CAIs with different rim types (higher for type II rims, lower for type I and III rims). Alternatively, olivine/gas ratios could have been constant (even zero), provided that the gas varied in composition from one object to another, with the most Si-rich vapor required to form spinel-poor, type III rims, and the most Mg-rich vapor required to form type II rims. These variations suggest that different rim types formed either in different local environments or at different times in an evolving system.

Model results suggest that nonsolar gas compositions and environments rich in olivine dust may have been involved in forming some rim types. To form clinopyroxene + anorthite-rich rims (type III), a vapor that is more Si-rich ($mg < 0.48$) than solar ($mg \approx 0.51$) is required, and to form spinel-free rims of this type, an even more Si-rich vapor ($mg < 0.28$) is required. For some olivine-rich rims (type II), either a nonsolar gas composition or a solar gas composition with high proportions of olivine dust is required. For example, the range of inferred conditions for producing the type II rim of Leo-1 is shown in Figure 9. In this figure, L ratios of unity are assumed, but different L ratios do not appreciably change the results except for very low values ($\ll 0.1$) of L_{MgMg}/L_{SiSi} or L_{CaCa}/L_{SiSi} . The external medium reacting with Leo-1 could have consisted of pure gas, if the gas were relatively Mg-rich ($mg \approx 0.59$) (Figure 9). Alternatively, the gas could have had a solar mg value (≈ 0.51), if the external medium was exceptionally dusty, with a molar (olivine dust)/gas ratio ≈ 0.4 (Figure 9). In an unfractionated nebular system the abundance of hydrogen is so high that the (silicate dust)/gas ratios will always be very low ($\approx 10^{-4}$), even if all silicates in the system (not just

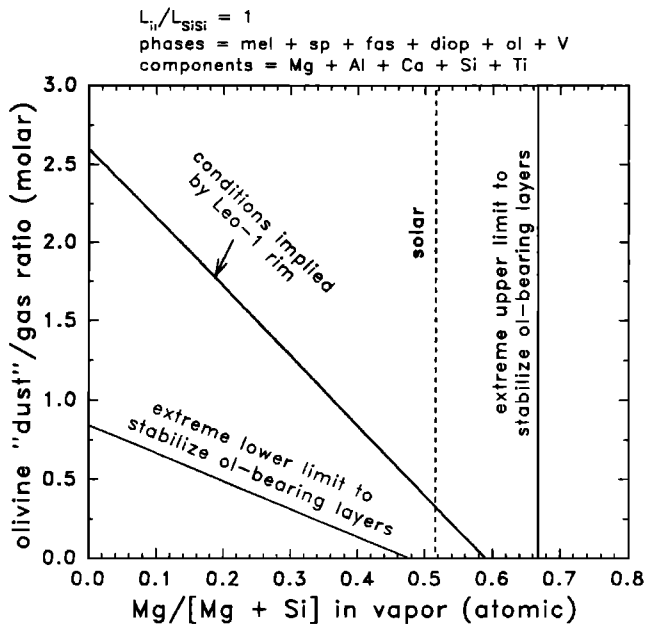


Figure 9. Vapor compositions and olivine dust/gas ratios in the external medium inferred from the rim of Leo-1. The curve labeled "conditions implied by Leo-1 rim" shows the locus of conditions in which the width of the diop+ol zone equals the width of the adjacent sp+diop zone in the Leo-1 model rim analogue CAI | mel+sp | sp+diop | diop+ol | vapor+ol, based on the observation that the width of the clinopyroxene + olivine zone is roughly equal to the width of the spinel + clinopyroxene zone in the Leo-1 rim (Table 3b). L ratios of unity were assumed.

olivine) are condensed. Thus the external medium reacting with Leo-1 would have to have been dust-enriched (by a factor of $\approx 10^4$) relative to an unfractionated nebula. Whether nonsolar gas compositions or high dust/gas ratios were involved, it appears that Leo-1 reacted with an environment that was chemically fractionated compared to solar composition.

What processes can explain the inferred gas compositions and dust/gas ratios? Two processes that could have been important in a nebular setting are (1) the condensation of silicate phases, especially olivine, from a gas either of solar or nonsolar initial composition, and (2) vaporization of silicates to form a vapor with non-solar composition.

Condensation of forsteritic olivine could have played an important role in rim formation because this phase is both stable and abundant in a variety of plausible nebular environments [e.g., *Wood and Hashimoto, 1993*], and because the condensation of forsterite will dramatically change the mg ratio of the remaining gas. For example, in an initially unfractionated (solar composition) system, forsterite condensation will drive the mg value of the gas from ≈ 0.5 to ≈ 0.1 [*Wood and Hashimoto, 1993*], which is well within the range implied for most rims. Condensation of forsterite would also produce grains that could accrete onto CAIs, but as previously discussed, high (olivine dust)/gas ratios cannot be produced in an unfractionated nebular system. Thus, while forsterite condensation can easily explain gas compositions more Si-rich than solar, it cannot also explain high dust/gas ratios unless the bulk system was enriched in a dust fraction.

Vaporization of previously condensed silicates may also have been important in rim formation. The gas produced by the

vaporization of silicates would tend to be oversaturated in silicate components relative to the unfractionated case, and this would ultimately lead to the condensation of larger amounts of dust at the same temperature [*Wood and Hashimoto, 1993*]. Consequently, potentially high (olivine dust)/gas ratios could be obtained. Based on experimental data, it appears that the composition of a vapor produced during vaporization will depend both on the composition of the starting material and on the relative volatilities of elements [*Notsu et al., 1978*]. Experiments by *Hashimoto [1983]* and *Notsu et al. [1978]* suggest that partial vaporization of material with initially solar, CV3 chondrite, or CAI-like compositions will produce gas compositions that are distinctly nonsolar ($mg < 0.51$) over a large range in vaporization extent (Figure 10). Partial vaporization of CAIs at their margins (during "flash heating") may have been the first step in rim formation to form refractory-element-enriched residues, and thus rim metasomatism may have occurred by the reaction of CAIs with the vapor that was produced during flash heating. Assuming a reasonable estimate of 60-90% vaporization of CAI margins during flash heating, a variety of gas compositions with mg values of ≈ 0.10 -0.45 could have been produced, depending on the composition of the CAIs (Figure 10). Such gas compositions are again within the range implied for rim formation.

Vaporization of CAIs or chondritic silicates would tend to produce a gas with an already less than solar mg ratio, and

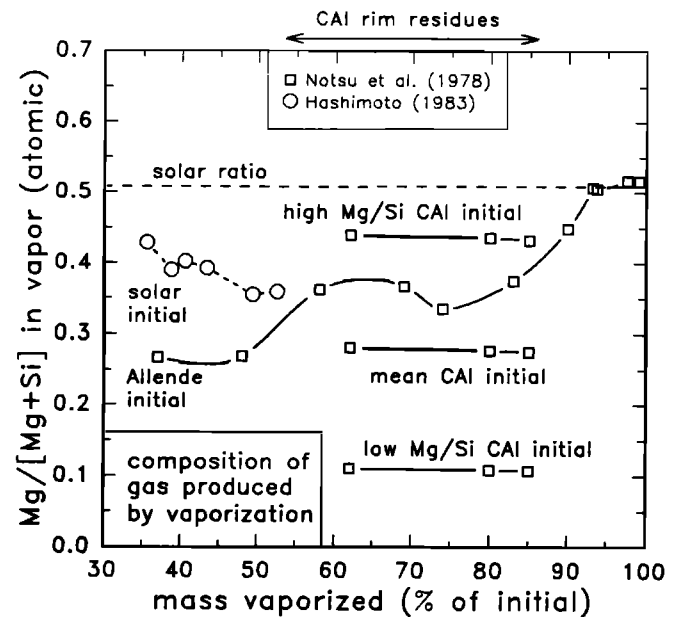


Figure 10. The mg (= $Mg/[Mg + Si]$ atomic) ratio in gas produced by vaporizing objects of various starting compositions, based on the vaporization data of *Notsu et al. [1978]* and *Hashimoto [1983]*. Gas compositions were inferred from changes in the compositions of vaporization residues produced in experiments and were calculated by taking the difference between the actual concentrations of Si and Mg in the residues and the theoretical concentrations these elements would have had if they behaved similarly to the most refractory major element in the residues (usually Al or Ti). The curves labeled "mean CAI," "high Mg/Si CAI," and "low Mg/Si CAI" refer to the vapor compositions produced by flash heating CAIs with the starting compositions of mean, high Mg/Si, and low Mg/Si coarse-grained CAIs in Vigarano, Leoville, and Efremovka [*Ruzicka, 1996*]. The expected gas compositions have $mg \leq$ solar.

subsequent condensation of olivine from the gas would drive the mg ratio of the gas even lower, while simultaneously producing olivine dust. This would produce a range of nonsolar, mainly Si-rich gas compositions, and a range of (olivine dust)/gas ratios, as condensation progressed. If CAIs were reacting with a dusty gas, while vaporization and condensation were occurring around them, the variety of rim types can be explained.

Conclusions

The overall layer structure and the major element zoning of clinopyroxene layers in CAI rims can be explained by quantitative layer growth models in which the layers formed by reaction and diffusion in a metasomatic process. During metasomatism, Mg and Si were introduced into CAIs to form the layers, and Mg isotopes were exchanged between the CAIs and their surroundings. The external medium appears to have consisted mainly of vapor (atomic Mg/[Mg+Si] \leq 0.66) and olivine-rich material. Differences in vapor compositions, or in (olivine dust)/gas ratios, were largely responsible for forming different rim types. Vapor compositions as Si-rich as Mg/[Mg+Si] \leq 0.28 may be required to form anorthite-rich, spinel-free rims, and olivine-rich rims may have formed in environments with high (olivine dust)/gas ratios. In one well-studied CAI, it appears that Mg isotope exchange and layer growth could have been initiated either in a short-duration (<10 hour) heating event at high temperature (>1450°C), or at lower temperatures (\leq 1450°C) by cooling at \leq 0.1-2°C/h.

Although the layer growth models are generally successful at explaining rim layers, there is evidence that they are oversimplified and that a complete quasi steady state condition was not achieved because of changes in pressure, temperature, or reactant composition during layer growth. Consequently, melilite was incompletely removed by reaction in some rims. Furthermore, most (\approx 50-97%) of the spinel in rims formed by some process other than metasomatism, and this "excess" spinel was also incompletely removed by reaction.

Based on the results of this study, the following scenario for rim formation is proposed. (1) Coarse-grained CAIs were flash heated to produce thin, refractory residues on their margins and a Mg-Si-rich vapor surrounding the CAIs. The residues consisted partly of spinel and partly of refractory melt that may have solidified into glass or one or more Ca-aluminate minerals as the CAIs began to cool. (2) The CAI interiors, their refractory coatings, and the vapor surrounding the CAIs immediately reacted with one another to remove refractory glass and Ca-aluminate minerals from the residues. Olivine grains may have begun to condense from the gas and accrete onto some CAI surfaces, and CAIs may have begun to exchange Mg isotopes with their surroundings. (3) Reaction and isotopic exchange between the CAIs and their surroundings continued as the objects cooled. This produced the compact mineral layers characteristic of rims by a coupled reaction-diffusion process, and the radial gradients in Mg-isotopic composition observed within the outer portions of some CAIs.

Acknowledgments. The author wishes to thank Bill Boynton for discussions about various aspects of this work, especially regarding rim-forming mechanisms and the implications of CAI-gas isotopic exchange; Carleton Moore, Glenn MacPherson, and Marty Prinz for loans of thin-sections containing the CAIs studied by the author; and Xin Hua, Alexander Krot, Melinda Hutson, and an anonymous reviewer for constructive comments regarding this manuscript that led to its improvement. This work was supported by NASA grant NAGW 3373 and NSF grant EAR 92-18857 to William V. Boynton.

References

- Ashworth, J.R., and J.J. Birdi, Diffusion modelling of coronas around olivine in an open system, *Geochim. Cosmochim. Acta*, **54**, 2389-2401, 1990.
- Beckett, J.R., and L. Grossman, Melting experiments on Allende coarse-grained compositions (abstract), *Lunar Planet. Sci.*, **XIII**, 31-32, 1982.
- Boynton, W.V., and D.A. Wark, Trace element abundances in rim layers of an Allende Type A coarse-grained, Ca,Al-rich inclusion (abstract), *Meteoritics*, **19**, 195, 1984.
- Boynton, W.V., and D.A. Wark, Refractory rims: Evidence for high temperature events in the post-formation history of Ca,Al-rich inclusions (abstract), *Meteoritics*, **20**, 613-614, 1985.
- Boynton, W.V., and D.A. Wark, Origin of CAI rims, I, The evidence from rare earth elements (abstract), *Lunar Planet. Sci.*, **XVIII**, 117-118, 1987.
- Brady, J.B., Reference frames and diffusion coefficients, *Am. J. Sci.*, **275**, 954-983, 1975.
- Davis, A.M., G.J. MacPherson, and R.W. Hinton, Rims revealed-- Ion microprobe analysis of individual rim layers in a Vigarano Type A inclusion (abstract), *Meteoritics*, **21**, 349-351, 1987.
- Fahey, A.J., E.K. Zinner, G. Crozaz, A.S. Kornacki, and A.A. Ulyanov, REE and isotopic studies of a coarse-grained CAI from Efremovka (abstract), *Meteoritics*, **20**, 643, 1985.
- Fahey, A.J., E.K. Zinner, G. Crozaz, and A.S. Kornacki, Microdistributions of Mg isotopes and REE abundances in a Type A calcium-aluminum-rich inclusion from Efremovka, *Geochim. Cosmochim. Acta*, **51**, 3215-3229, 1987.
- Fisher, G.W., Nonequilibrium thermodynamics as a model for diffusion-controlled processes, *Am. J. Sci.*, **272**, 897-924, 1973.
- Fisher, G.W., Nonequilibrium thermodynamics in metamorphism, in *Thermodynamics in Geology*, pp. 381-403, D. Reidel, Norwell, Mass., 1977.
- Fisher, G.W., Rate laws in metamorphism, *Geochim. Cosmochim. Acta*, **42**, 1035-1050, 1978.
- Fisher, G.W., and D. Elliot, Criteria for quasi-steady diffusion and local equilibrium in metamorphism, in *Geochemical Transport and Kinetics*, edited by H.S. Yoder Jr. and R.A. Yund, *Carnegie Inst. Washington Pub.*, **634**, 231-241, 1974.
- Fisher, G.W., and A.C. Lasaga, Irreversible thermodynamics in petrology, in *Kinetics of Geochemical Processes*, edited by A.C. Lasaga and R.J. Kirkpatrick, *Rev. Mineral.*, **8**, 171-209, 1981.
- Foster, C.T., Jr., A thermodynamic model of mineral segregations in the lower sillimanite zone near Rangely, Maine, *Am. Mineral.*, **66**, 260-277, 1981.
- Foster, C.T., Jr. The role of biotite as a catalyst in reaction mechanisms that form sillimanite, *Can. Mineral.*, **29**, 943-963, 1991.
- Ganguly, J., H. Yang, and S. Ghose, Thermal history of mesosiderites: Constraints from compositional zoning and Fe-Mg ordering in orthopyroxenes, *Geochim. Cosmochim. Acta*, **58**, 2711-2723, 1994.
- Goswami, J.N., G. Srinivasan, and A.A. Ulyanov, Ion microprobe studies of Efremovka CAIs: Magnesium isotope composition, *Geochim. Cosmochim. Acta*, **58**, 431-447, 1994.
- Grossman, L., Refractory inclusions in the Allende meteorite, *Annu. Rev. Earth Planet Sci.*, **8**, 559-608, 1980.
- Hartley, G.S., and J. Crank, Some fundamental definitions and concepts in diffusion processes, *Trans. Faraday Soc.*, **45**, 801-818, 1949.
- Hashimoto, A., Evaporation metamorphism in the early solar nebula-- Evaporation experiments on the melt FeO-MgO-SiO₂-CaO-Al₂O₃ and chemical fractionations of primitive materials, *Geochem. J.*, **17**, 111-145, 1983.
- Joesten, R., Evolution of mineral assemblage zoning in diffusion metasomatism, *Geochim. Cosmochim. Acta*, **41**, 649-670, 1977.
- Joesten, R., Local equilibrium in metasomatic processes revisited: Diffusion-controlled growth of chert nodule reaction rims in dolomite, *Am. Mineral.*, **76**, 743-755, 1991.
- Katchalsky, A., and P.F. Curran, *Nonequilibrium Thermodynamics in Biophysics*, 248 pp., Harvard Univ. Press, Cambridge, Mass., 1965.
- Kress, V.C., and M.S. Ghiorso, Multicomponent diffusion in MgO-Al₂O₃-SiO₂ and CaO-MgO-Al₂O₃-SiO₂ melts, *Geochim. Cosmochim. Acta*, **57**, 4453-4466, 1993.
- Lee, T., Implications of isotopic anomalies for nucleosynthesis, in *Meteorites and the Early Solar System*, edited by J.F. Kerridge and M.S. Matthews, pp. 1063-1089, Univ. of Ariz. Press, Tucson, 1988.
- Lorin, J.-C., M. C.-Michel-Lévy, and C. Desnoyers, Ophitic Ca-Al-rich inclusions in the Allende and Leoville meteorites: A petrographic and ion microprobe study, *Meteoritics*, **13**, 537-540, 1978.

- MacPherson, G.J., L. Grossman, J.M. Allen, and J.R. Beckett., Origin of rims on coarse-grained inclusions in the Allende meteorite, *Proc. Lunar Planet. Sci. Conf.*, 12th, 1079-1091, 1981.
- MacPherson, G.J., J.M. Paque, E. Stolper, and L. Grossman, The origin and significance of reverse zoning in melilite from Allende Type B inclusions, *J. Geol.*, 92, 289-305, 1984.
- MacPherson, G.J., R.W. Hinton, and A.M. Davis, Petrology, chemistry and magnesium isotope systematics of a unique Allende inclusion (abstract), *Meteoritics*, 21, 439, 1986.
- MacPherson, G.J., D.A. Wark, and J.T. Armstrong, Primitive material surviving in chondrites: Refractory inclusions, in *Meteorites and the Early Solar System*, edited by J.F. Kerridge and M.S. Matthews, pp. 746-807, Univ. of Ariz. Press, Tucson, 1988.
- McSween, H.Y., Jr., Petrographic variations among carbonaceous chondrites of the Vigarano type, *Geochim. Cosmochim. Acta*, 41, 1777-1790, 1977.
- Morioka, M., and H. Nagasawa, Diffusion in single crystals of melilite, II, Cations, *Geochim. Cosmochim. Acta*, 55, 751-759, 1991.
- Murrell, M.T., and D.S. Burnett., Spinel-perovskite rims: Constraints on the thermal histories of Ca-Al-rich inclusions (abstract), *Lunar Planet. Sci.*, XVII, 589-590, 1986.
- Murrell, M.T., and D.S. Burnett, Actinide chemistry in Allende Ca-Al-rich inclusions, *Geochim. Cosmochim. Acta*, 51, 985-999, 1987.
- Nishiyama, T., Steady diffusion model for olivine-plagioclase corona growth, *Geochim. Cosmochim. Acta*, 47, 283-294, 1983.
- Notsu, K., N. Onuma, and N. Nishida, High temperature heating of the Allende chondrite, *Geochim. Cosmochim. Acta*, 42, 903-907, 1978.
- Paque, J.M., and E. Stolper, Experimental evidence for slow cooling of Type B CAIs from a partially molten state (abstract), *Lunar Planet. Sci.*, XIV, 596-597, 1983.
- Ruzicka, A., Petrologic-kinetic studies of meteorites, Ph.D. dissertation, 300 pp., Lunar and Planet. Lab., Dep. of Planet. Sci., Univ. of Arizona, Tucson, 1996.
- Ruzicka, A., and W.V. Boynton, Microfaulting of CAI rim layers and relationship to the fabric of the Leoville (CV3) chondrite (abstract), *Lunar Planet. Sci.*, XIII, 1191-1192, 1992.
- Ruzicka, A., and W.V. Boynton, The anatomy and bulk composition of CAI rims in the Vigarano (CV3) chondrite (abstract), *Meteoritics*, 28, 426, 1993.
- Ruzicka, A., and W.V. Boynton, Origin of CAI rims by vaporization and metasomatism (abstract), *Meteoritics*, 29, 526, 1994.
- Ruzicka, A., W.V. Boynton, and J. Ganguly, Olivine coronas, metamorphism, and the thermal history of the Morristown and Emery mesosiderites, *Geochim. Cosmochim. Acta*, 58, 2725-2741, 1994.
- Sheng, Y.J., G.J. Wasserburg, and I.D. Hutcheon, Self-diffusion of magnesium in spinel and in equilibrium melts, *Geochim. Cosmochim. Acta*, 56, 2535-2546, 1992.
- Stolper, E., and J.M. Paque, Crystallization sequences of Ca-Al-rich inclusions from Allende: The effects of cooling rate and maximum temperature, *Geochim. Cosmochim. Acta*, 50, 1785-1806, 1986.
- Swapp, S.M., Mass transfer and coupled reactions in low grade metamorphism of calcareous concretions, *Am. J. Sci.*, 286, 433-462, 1988.
- Tilton, G.R., Age of the solar system, in *Meteorites and the Early Solar System*, edited by J.F. Kerridge and M.S. Matthews, pp. 259-275, Univ. of Ariz. Press, Tucson, 1988.
- Wark, D.A., and W.V. Boynton, Origin of CAI rims, II, The evidence from refractory metals, major elements and mineralogy (abstract), *Lunar Planet. Sci.*, XVIII, 1054-1055, 1987.
- Wark, D.A., and J.F. Lovering, Marker events in the early evolution of the solar system: Evidence from rims on Ca-Al-rich inclusions in carbonaceous chondrites, *Proc. Lunar Sci. Conf.*, 8th, 95-112, 1977.
- Wark, D.A., B. Spettel, H. Palme, and A. El Goresy, Rim formation by flash heating and metasomatism: evidence from Vigarano CAI VI-1 (abstract), *Lunar Planet. Sci.*, XIX, 1230-1231, 1988.
- Wood, J.A., and A. Hashimoto, Mineral equilibrium in fractionated nebular systems, *Geochim. Cosmochim. Acta*, 57, 2377-2388, 1993.

A. Ruzicka, Planetary Geosciences Institute, Department of Geological Sciences, University of Tennessee, Knoxville, TN 37996 (email: aruzicka@utk.edu)

(Received February 6, 1996; revised January 28, 1997; accepted February 10, 1997.)